

Marine Carbohydrates and Other Sea Spray Aerosol Constituents Across Altitudes in the Lower Troposphere of Ny-Ålesund, Svalbard

Sebastian Zeppenfeld^{1*}, Jonas Schaefer², Christian Pilz², Kerstin Ebell³, Moritz Zeising⁴, Frank Stratmann², Holger Siebert², Birgit Wehner², Matthias Wietz^{4,5,6}, Astrid Bracher^{4,7}, and Manuela van Pinxteren¹

1 Atmospheric Chemistry Department (ACD), Leibniz Institute for Tropospheric Research (TROPOS), Leipzig, Germany

2 Atmospheric Microphysics (AMP), Leibniz Institute for Tropospheric Research (TROPOS), Leipzig, Germany

3 Institute for Geophysics and Meteorology, University of Cologne, Cologne, Germany

4 Alfred Wegener Institute Helmholtz Centre for Polar and Marine Research, Bremerhaven, Germany

5 Max Planck Institute for Marine Microbiology, Bremen, Germany

6 Institute for Chemistry and Biology of the Marine Environment, University of Oldenburg, Oldenburg, Germany

7 Institute of Environmental Physics, University of Bremen, Bremen, Germany

*Correspondence to: Sebastian Zeppenfeld (zeppenfeld@tropos.de)

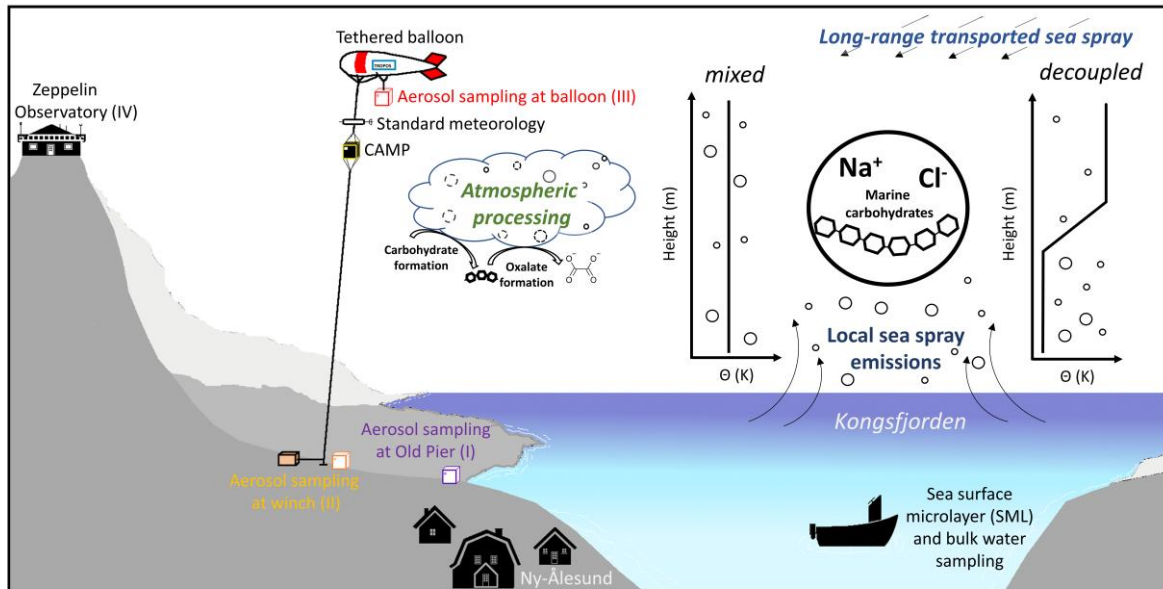
Abstract

Marine combined carbohydrates in aerosol particles (CCHO_{aer}) have the potential to influence cloud formation and properties, but it remains unclear to what extent they reach altitudes relevant for cloud processes. Balloon-borne measurements of major sea spray aerosol (SSA) constituents, including sodium (Na⁺_{aer}) and CCHO_{aer}, were conducted in autumn 2021 and spring 2022 in Ny-Ålesund (Svalbard). Total suspended particles were collected at 321–1112 m, covering both the marine boundary layer and the free troposphere, with Na⁺_{aer} ranging 23–850 ng m⁻³ and CCHO_{aer} 3.8–274 ng m⁻³. The chemical composition of balloon-borne aerosol samples was compared with synchronized ground level measurements at the balloon's winch (Na⁺_{aer}: 35–3710 ng m⁻³; CCHO_{aer}: 1.9–194 ng m⁻³), and at the Old Pier (Na⁺_{aer}: 140–1470 ng m⁻³; CCHO_{aer}: 1.6–10.0 ng m⁻³), where freshly emitted SSA particles were sampled. Surface seawater from the Kongsfjorden was analyzed to evaluate the sea-air transfer of marine CCHO. Air mass histories, atmospheric mixing, and cloud conditions were evaluated for three selected cases to explain vertical concentration patterns. A strong correlation (R=0.78, p<0.001) between combined xylose (<0.2–14.1 ng m⁻³) in CCHO_{aer} and oxalate_{aer} (<1–67 ng m⁻³) across all altitudes, suggests either coproduction or a connection through atmospheric

36 processing. These results provide a first comprehensive picture of how local primary sea-air
37 transfer of marine combined carbohydrates, long-range transport, in-situ formation, and
38 atmospheric processing together shape their distribution.

39

40



41

42 **1. Introduction**

43 Aerosol particles in the High Arctic atmosphere originate from a complex interplay of primary
44 and secondary emissions from oceanic, terrestrial, cryospheric, and anthropogenic sources,
45 followed by diverse atmospheric processes (Schmale et al., 2021). They play a crucial role in
46 the radiation balance, directly by scattering and absorbing shortwave and longwave radiation,
47 and indirectly by influencing cloud formation and phase state as cloud condensation nuclei
48 and ice-nucleating particles (Lohmann and Feichter, 2005; Penner et al., 2001; Quinn et al.,
49 2015; Yu et al., 2006). These effects are strongly governed by the particles' size distribution
50 and chemical composition (Dusek et al., 2006; Farmer et al., 2015; Kanji et al., 2017; Pilinis et
51 al., 1995).

52 The High Arctic predominantly consists of marine areas, characterized by a seasonally variable
53 extent of sea ice cover and open waters. Consequently, sea spray aerosol (SSA) particles
54 represent a key group of primary aerosol particles in this region (Heutte et al., 2025; Kang et
55 al., 2025; Schmale et al., 2022). As Arctic sea ice coverage continues to decline due to global
56 warming, enhanced by Arctic amplification (Cai et al., 2021; Francis and Wu, 2020; Wendisch
57 et al., 2017, 2023), larger expanses of open ocean are anticipated to become significant
58 sources of SSA emissions (Browse et al., 2014; Struthers et al., 2011). Although direct
59 measurements remain sparse, Sharma et al. (2019) readily observed increasing sea salt
60 aerosol production from sea spray over 34 years at the Arctic air chemistry observatory in
61 Alert, Canada.

62 SSA particles are generated through wind-driven wave action, which causes bubbles at the sea
63 surface to burst, ejecting film and jet droplets into the atmosphere (Veron, 2015). SSA
64 particles primarily consist of inorganic sea salt ions, mainly sodium and chloride, along with
65 organic matter (OM), including significant amounts of marine carbohydrates originating from
66 the sea surface microlayer (SML) and the underlying bulk seawater (Müller et al., 2010; van
67 Pinxteren et al., 2023; Quinn et al., 2015; Russell et al., 2010). In seawater, carbohydrates are
68 produced by photoautotrophic organisms, predominantly as linear or branched oligo- and
69 polysaccharides (Aluwihare et al., 1997; Borch and Kirchman, 1997; Engel and Händel, 2011;
70 Khadem, 2012), collectively referred to as combined carbohydrates (CCHO). They also exist as
71 monosaccharides, known as dissolved free carbohydrates. Both fractions are consumed or
72 transformed by heterotrophic organisms, with turnover rates largely determined by their

73 molecular structure and composition (Arnosti et al., 2021; Engel and Händel, 2011; Ittekkot et
74 al., 1981; Kirchman et al., 2001).

75 Sodium in aerosol particles (Na^+_{aer}) is highly abundant in the marine boundary layer, with only
76 minor terrestrial sources and greater atmospheric stability compared to chloride (Cl^-_{aer}) (Chi
77 et al., 2015; Keene et al., 1986; Manders et al., 2010; Sander et al., 2003). This makes it a
78 valuable conservative tracer for studying the sea-to-air transfer and atmospheric
79 transformation of organic compounds, including marine carbohydrates, as well as other
80 inorganic SSA constituents. Notably, the ratio of OM to Na^+ is significantly higher in SSA
81 particles than in seawater, reflecting not only the preferential enrichment of surface-active
82 substances at the interface but also a more complex interplay of factors such as water
83 solubility, biological activity within the ocean surface, and co-adsorption processes involving
84 matrix constituents (Burrows et al., 2014; Gantt et al., 2011; Hasenecz et al., 2020, 2019;
85 Hoffman and Duce, 1976; Jayarathne et al., 2016; van Pinxteren et al., 2017; Quinn et al., 2015;
86 Russell et al., 2010; Schill et al., 2018). This enrichment is particularly pronounced in
87 submicron particles compared to supermicron particles. Furthermore, following the sea-to-air
88 transfer of OM and CCHO, recent laboratory (Hasenecz et al., 2020; Malfatti et al., 2019) and
89 field (Zeppenfeld et al., 2021, 2023) observations suggest their molecular transformation or
90 additional in-situ formation, driven by abiotic, microbial or enzymatic activities in the
91 atmosphere.

92 SSA particles are known to function as both cloud condensation nuclei (Orellana et al., 2011;
93 Xu et al., 2022) and ice-nucleating particles (Alpert et al., 2022; DeMott et al., 2016; Hill et al.,
94 2023; Mirrielees et al., 2024), underscoring their important role in cloud microphysics, cloud
95 formation, and precipitation processes. Recently, Hartmann et al. (2025) demonstrated,
96 through a combination of lab and field data, that SSA particles' ice-nucleating activity is likely
97 attributable to the polysaccharides they contain. Model simulations further indicated that the
98 ice-nucleating activity of marine polysaccharides is particularly significant within the
99 temperature range between -20 and -15°C in remote oceanic regions, where contributions
100 from terrestrial ice-nucleating particles are minimal or absent. Furthermore, Rocchi et al.,
101 (2024) demonstrated that the presence of glucose-rich CCHO, in combination with sea salt,
102 significantly enhances SSA production in eastern Arctic waters. This finding may improve the
103 predictability of SSA emissions in marine models.

104 In the field, marine combined carbohydrates in aerosol particles (CCHO_{aer}) have been
105 predominantly measured at ship-based or coastal locations, which are in close proximity to
106 local marine emission sources both horizontally and vertically (Leck et al., 2013; van Pinxteren
107 et al., 2023; Zeppenfeld et al., 2021, 2023). In contrast, only a few studies have investigated
108 CCHO_{aer} (Karl et al., 2019; Yttri et al., 2024) at an elevated mountain site in a marine-influenced
109 setting, aiming to assess atmospheric concentrations at higher altitudes. Vertically resolved
110 field data comparing ground-level and elevated altitudes using mobile platforms for marine
111 CCHO_{aer} have, however, been lacking to date. This is due to several methodological challenges,
112 most fundamentally the absence of suitable high-resolution online detection techniques for
113 CCHO_{aer}, reflecting the inherent analytical difficulty of this compound class. As a consequence,
114 current approaches rely on offline analyses, which are further constrained by low atmospheric
115 concentrations that approach their detection limits. In addition, lightweight yet powerful high-
116 flow pumps remain technically challenging to realize for mobile airborne platforms (e.g.,
117 drones or balloon-based systems), where payload and power constraints limit the collection
118 of sufficient aerosol mass during short sampling periods. As a result, it remains unclear to what
119 extent and under which conditions CCHO_{aer} reach the upper marine boundary layer and the
120 free troposphere, leaving high uncertainty about the broader relevance of these biomolecules
121 for cloud formation and glaciation beyond controlled laboratory conditions.

122 Previous airborne measurements around Svalbard (Hara et al., 2003; Simon et al., 2025) and
123 the Canadian Arctic (Köllner et al., 2017) demonstrated that SSA particles, identified by Na⁺
124 and Cl⁻, are present in higher altitudes of the lower troposphere, and, to a lesser extent, reach
125 the middle free troposphere (3–6 km a.s.l.). Some of these aerosol particles showed signs of
126 atmospheric aging, such as the replacement of chloride with nitrate and sulfate in the SSA
127 particles. While vertically resolved data exists for major inorganic SSA constituents, such
128 extended information is lacking for marine CCHO_{aer}.

129 Recent methodological advances now allow for a more detailed investigation of the transport
130 mechanisms and atmospheric chemical fate of marine carbohydrates. In this study, we
131 present atmospheric concentrations of these biomolecules alongside common inorganic SSA
132 constituents. Measurements were conducted from ground level up to various altitudes within
133 the boundary layer and lower free troposphere using a tethered helium balloon in Ny-Ålesund
134 on Svalbard during autumn 2021 and spring 2022. For selected cases, we examined the
135 influence of mixing state, meteorological conditions, and air mass history on the observed

136 aerosol composition. Finally, this study addresses the potential atmospheric processing and
137 transformation of marine carbohydrates, with a focus on their possible contribution to
138 secondary aerosol formation and their implications for atmospheric chemistry and cloud-
139 relevant processes.

140 2. Methods

141 This section summarizes the observational and modelling approaches used in this work. It
 142 covers the study area, field sampling, offline and online measurements, supporting datasets,
 143 model calculations, and statistical and visualization methods for data interpretation. An
 144 overview of all relevant parameters and methods is provided in **Table 1**.

145 **Table 1.** Overview of parameters, methods and sample/media types used in this study.

| Category | Parameters | Method/Instrument/Model | Sample/Medium |
|---------------------------------|---|---|---|
| Major cations and anions | Na ⁺ , K ⁺ , Mg ²⁺ , Ca ²⁺ , Cl ⁻ , SO ₄ ²⁻ , oxalate | Ion chromatography | Bulk seawater, SML, aerosol particles (filter) |
| Free and combined carbohydrates | Fuc, Rha, Ara, Gal, Glc, Xyl, Man, Fru, GalN, GlcN, MurAc, GalAc, GlcAc | HPAEC-PAD | Bulk seawater, SML, aerosol particles (filter) |
| Sea surface temperature | SST | Digital Thermometer | Ocean surface |
| Aerosol number concentration | N ₁₅₀ (150-2900 nm) | POPS (CAMP) | Atmospheric column |
| Meteorology | T, U, WD, RH, p, wind, θ, q | Standard meteorology package + thermodynamic equations | Atmosphere at ground (AWIPEV), atmospheric column |
| Cloud properties | Clouds and hydrometer types, IWP, LWP, IWV | Cloudnet + HATPRO | Atmospheric column |
| Biogeochemistry (model) | TChl-a, dissolved acidic polysaccharides | FESOM2.1-REcoM3 | Ocean surface |
| Air mass origin | 48-h back-trajectories | NOAA HYSPLIT | Several altitudes of atmosphere |

146

147 2.1 Study area: Ny-Ålesund as an atmospheric observation site

148 Ny-Ålesund, located at 78.9°N at the Kongsfjorden in Svalbard (Norway), belongs to the
 149 world's northernmost permanently inhabited settlements with a year-round accessibility. It
 150 serves as a key research site for studying Arctic climate change and Arctic amplification. Ny-

151 Ålesund hosts long-term monitoring sites for aerosols and meteorology, such as the Zeppelin
152 Observatory (Platt et al., 2022), Gruvebadet (Amore et al., 2022), and the AWIPEV Observatory
153 (Maturilli et al., 2013, 2015). These, along with additional research stations operated by
154 various international institutions, provide valuable data for both long-term atmospheric
155 studies and short-term investigations like the present one.

156 However, Ny-Ålesund is not representative of the entire High Arctic. Its distinct topography,
157 situated within a fjord and surrounded by high mountains up to 800 m, leads to complex
158 atmospheric dynamics, including foehn-like effects (Shestakova et al., 2021). The local
159 boundary layer is relatively shallow characterized by an average mixing layer height below
160 700 m and a strong influence by orographic effects (Chang et al., 2017; Dekhtyareva et al.,
161 2018; Gierens et al., 2020). While free-tropospheric winds are predominantly westerly,
162 surface winds result from an interplay of land-sea breeze circulations, southeasterly
163 channeled winds along the fjord axis, and katabatic flows from the Zeppelin mountain range,
164 the Broeggerbreen glacier, or the Kongsvegen glacier (Esau and Repina, 2012; Gierens et al.,
165 2020). Additionally, large wind shear has been observed to generate turbulence, leading to
166 frequent neutral stratification (Gierens et al., 2020). Furthermore, boundary layer mixing can
167 occur even under a positive potential temperature gradient that would typically indicate
168 stable stratification. During the present field campaign, we observed that near-surface winds
169 often shift unpredictably, changing direction without a clear pattern, making airflow dynamics
170 challenging to interpret.

171 From an oceanographic perspective, Svalbard is similarly exceptional. The region is influenced
172 by the cold Arctic waters of the Spitsbergen Polar Current and the warm waters of the West
173 Spitsbergen Current (Feltracco et al., 2021). Kongsfjorden, located on the western coast of
174 Spitsbergen, lies at the interface of High Arctic and Atlantic influences, making it a dynamic
175 and variable environment (Bischof et al., 2019).

176 Therefore, findings from Ny-Ålesund may not be fully transferable to atmospheric processes
177 over sea ice or the open ocean in the High Arctic. However, in general, the representativeness
178 of any single Arctic site is highly questionable, as Freud et al., (2017) found significant
179 heterogeneity in aerosol particle size distribution across all Arctic sites in their study.

180 **2.2 Field sampling**

181 The field samples (aerosol particles, bulk seawater and SML) for this study were collected near
182 Ny-Ålesund and from the adjacent Kongsfjorden during autumn 2021 and spring 2022.

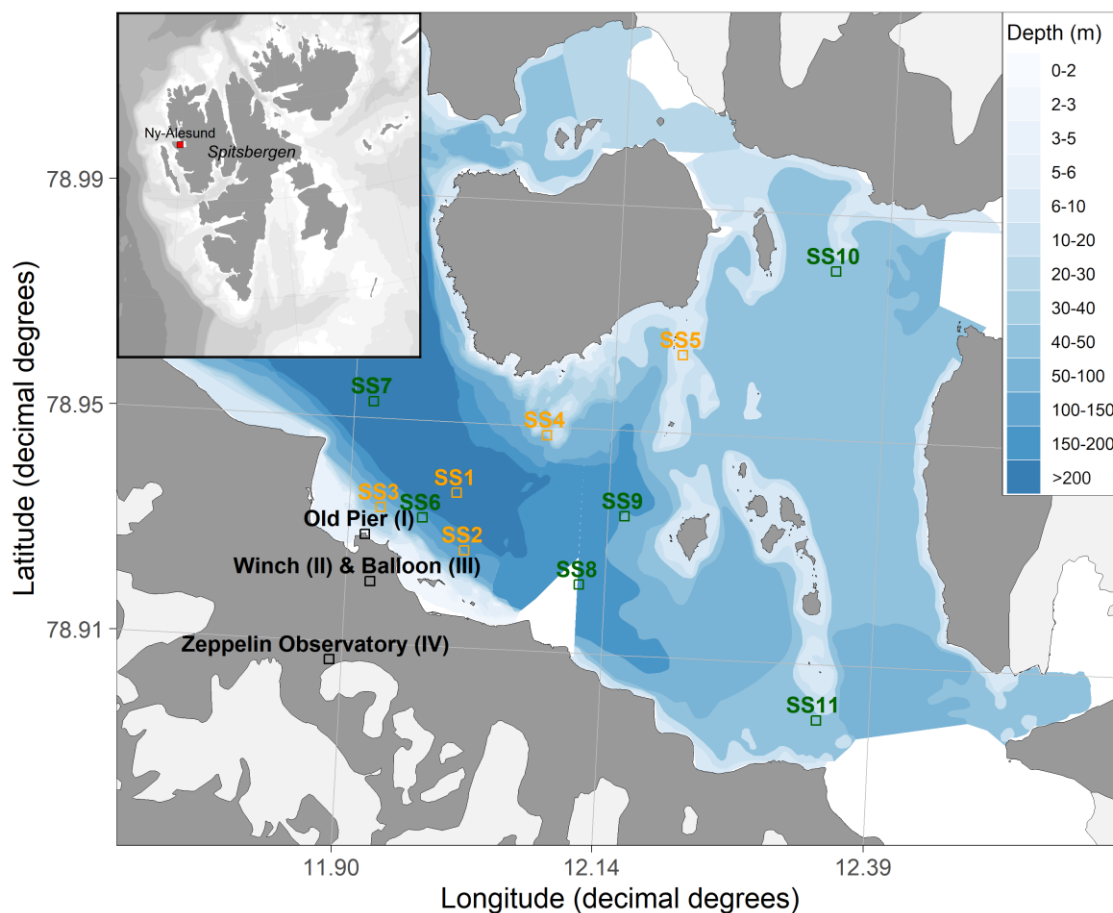


Figure 1. Map of the sampling locations. Aerosol particles were collected at: (I) the Old Pier, representing fresh SSA emissions; (II) the winch, representing ground measurements; (III) the tethered balloon at various altitudes; and (IV) the Zeppelin Observatory, serving as a reference for comparison. Bulk and SML samples were collected from different locations within Kongsfjorden. Orange squares (SS1-SS5) indicate autumn 2021 samples, while green squares (SS6-SS11) represent spring 2022 samples. Blue shading indicates water depth.

183

184 *a) Bulk seawater and SML sampling*

185 In total, 11 bulk surface seawater and 11 SML samples were taken from a small boat at various
186 dates and locations across the Kongsfjorden (**Figure 1, Table S1**). Bulk water samples were
187 obtained from a depth of 1 m using low-density polyethylene (LDPE) bottles secured to a
188 telescopic rod. The corresponding SML samples were collected using the glass plate technique
189 (Cunliffe and Wurl, 2014; van Pinxteren et al., 2012). A glass plate measuring
190 50 cm × 20 cm × 0.5 cm, with an oval sampling area of 2000 cm², was immersed vertically into

191 the surface of the fjord seawater and withdrawn at a steady rate of 15 cm s^{-1} . The SML film
192 attached to the glass surface was drained into a precleaned wide-neck plastic bottle using a
193 funnel and a framed Teflon wiper. Water samples were filtered through $0.2 \text{ }\mu\text{m}$ polycarbonate
194 filters (Whatman® Nuclepore™, 47 mm diameter) to separate dissolved and particulate
195 fractions. The filtrate, filters and field blanks were preserved at -20°C until chemical analyses
196 (inorganic ions, carbohydrates). Sea surface temperature (SST) was measured directly from
197 the boat at a depth of approximately 10 cm using a digital thermometer.

198 *b) Aerosol particle sampling in the surroundings of Ny-Ålesund*

199 Total suspended aerosol particles (TSP) were captured on polycarbonate filters ($0.8 \text{ }\mu\text{m}$,
200 Whatman® Nuclepore™, 47 mm diameter) at four locations (**Figure 1**): (I) Near the Old Pier
201 next to Kongsfjorden (8 samples), representing fresh SSA emissions; (II) near the balloon winch
202 close to the AWIPEV Observatory (17 samples), representing ground measurements; (III) at
203 high altitudes at the tethered balloon (14 samples); and (IV) at the Zeppelin Observatory
204 (1 sample), serving as a reference for comparison. **Table S2** provides details of individual
205 aerosol particle samplings near the Old Pier (I), while **Table S3** presents the sampling times,
206 locations and heights of all the individual high-altitude aerosol samples (III & IV), along with
207 the corresponding simultaneous ground-level samples (II) taken near the winch.

208 For sampling aerosol particles at the Old Pier (4 m above sea level), a filter holder with a
209 polycarbonate filter attached to a pump was used. Sampling lasted between 4 and 7 days.
210 Flow rates, measured at the beginning and the ending of the sampling with a flowmeter,
211 ranged from 5 to 10 L min^{-1} , with total air volumes between 44 and 82 m^3 . The estimated
212 diameter-dependent collection efficiency of this TSP sampling setup, assuming a 90°
213 aspiration angle, is shown in **Figure S1**. To reduce the risk of pump failure due to cold
214 temperatures or snow, the pumps were housed in a Zarges box for protection.

215 High-altitude TSP samples were collected using the helium-filled tethered balloon BELUGA, as
216 described in detail by Pilz et al. (2023). The balloon's altitude was controlled using an electric
217 winch located near the AWIPEV Observatory, with ascent and descent rates from 1 to 3 m s^{-1} .
218 The tethered balloon operated under various meteorological conditions, including both clear
219 and cloudy skies. At a specified altitude, a HALFBAC (High-volume And Light-weight Filter
220 sampler for BALloon-borne appliCation) (Grawe et al., 2023) collected aerosol particles 2-3 m
221 below the balloon. The HALFBAC is a custom-designed, lightweight aerosol particle sampler

222 operating at a pump flow rate between 25 and 35 L min⁻¹. It is capable of collecting sufficient
223 aerosol mass on filters at high altitudes for subsequent offline chemical and microphysical
224 analyses. Simultaneously, another HALFBAC collected ground-level aerosol particles near the
225 electric winch (20 m above sea level). Additionally, one aerosol sample (Filter ID 62, sampling
226 date: 10/05/2022) was collected at the Zeppelin Observatory, a permanent monitoring station
227 located at 474 m a.s.l. on Zeppelinfjellet, using the HALFBAC. Synchronized aerosol particle
228 sampling at the winch and the balloon typically lasted around two hours, as detailed in **Table**
229 **S3**. The collection efficiency for TSP sampling using HALFBAC is discussed in the supplement
230 (A1) and **Figure S1**.

231

232 **2.3 Chemical analyses from offline aerosol particle filters and seawater**

233 For the analysis of major cations, anions and marine carbohydrates in aerosol particles, the
234 complete polycarbonate filters were extracted in 6-7 mL of ultrapure water
235 (resistivity > 18.2 MΩ) for two hours followed by a filtration through a 0.45 μm syringe filter.
236 Frozen seawater samples were thawed at 4°C in a refrigerator one day before analysis.

237 *a) Major cations and anions*

238 Major inorganic ions, including sodium (Na⁺), potassium (K⁺), magnesium (Mg²⁺), calcium
239 (Ca²⁺), chloride (Cl⁻), sulfate (SO₄²⁻), and oxalate, were quantified in 0.45 μm filtered aqueous
240 aerosol extracts, bulk seawater and SML samples using ion chromatography (Dionex ICS-6000,
241 Thermo Scientific) as described by Zeppenfeld et al. (2021). For both cations and anions, the
242 injection volume was 10 μL. Cations were separated isocratically using a 36 mM
243 methanesulfonic acid eluent at a flow rate of 0.16 mL min⁻¹ on a Dionex IonPac CS16 (2 mm ×
244 250 mm) column with a CG16 guard column (2 mm × 50 mm). Anions were separated on a
245 Dionex IonPac AS18 column (2 mm × 250 mm) with an AG18 guard column (2 mm × 50 mm),
246 using a potassium hydroxide (KOH) gradient elution at 0.3 mL min⁻¹. The gradient started at 4
247 mM KOH (0–4 min), increased to 20 mM (up to 8 min), then to 28 mM (up to 13.5 min), held
248 at 28 mM until 17.4 min, increased to 40 mM (up to 21.5 min), followed by a step to 80 mM
249 (up to 23.5 min), before returning to 4 mM KOH.

250 Both systems used suppressors (Dionex ADRS600 2 mm for anions and Dionex CDRS600 2 mm
251 for cations). Analytical uncertainty for each ion was below 5%. Aerosol extracts were

252 measured undiluted, while bulk seawater and SML samples were analyzed at a 1:15,000
253 dilution.

254 *b) Dissolved free and combined carbohydrates*

255 Carbohydrates in seawater and aerosol particle extracts were measured according to the
256 protocols outlined by Zeppenfeld et al. (2020, 2021), utilizing high-performance anion-
257 exchange chromatography with pulsed amperometric detection (HPAEC-PAD). The system
258 was equipped with a Dionex CarboPac PA20 analytical column (3 mm × 150 mm) and a Dionex
259 CarboPac PA20 guard column (3 mm × 30 mm). The applied eluent gradient separated the
260 following monosaccharide units: fucose (Fuc), rhamnose (Rha), arabinose (Ara), galactose
261 (Gal), glucose (Glc), xylose (Xyl), mannose (Man), fructose (Fru), galactosamine (GalN),
262 glucosamine (GlcN), muramic acid (MurAc), galacturonic acid (GalAc), and glucuronic acid
263 (GlcAc). The analytical uncertainty for each monosaccharide was below 10%. Dissolved free
264 carbohydrates were measured without hydrolysis, whereas CCHO include those
265 monosaccharides released by acid hydrolysis (0.8 M HCl, 100°C, 20 h). For seawater samples,
266 particulate combined carbohydrates (pCCHO, >0.2 µm) were measured from 0.2 µm
267 polycarbonate filters, while dissolved combined carbohydrates (dCCHO, <0.2 µm) were
268 measured from the filtrate after desalination via electrodialysis. Both fractions were later
269 summed to represent the total CCHO. For the winch and balloon samples, the limited air
270 volume and resulting low aerosol mass collected on the filters permitted quantification only
271 of the major monosaccharides (typically Glc, Xyl, Gal, Ara), while minor monosaccharides
272 remained largely below the instrumental detection limits. In contrast, samples from the Old
273 Pier and surface seawater provided sufficient analyte mass to quantify the full suite of the
274 CCHO monosaccharides.

275

276 **2.4 Vertical profiles from online measurements**

277 *a) Size-resolved aerosol particles number concentrations*

278 An optical particles size spectrometer (POPS, Handix), integrated into the Cubic Aerosol
279 Measurement Platform (CAMP) as described by Pilz et al. (2022), provided the integrated total
280 number concentrations (N_{150}) for aerosol particles between 150 and 2900 nm at a temporal
281 resolution of 1 second. On selected dates of HALFBAC sampling, CAMP was operated

282 simultaneously 25 m below the balloon providing insight into the vertical profile of N_{150} during
283 specific events. Vertical profiles are presented as rolling averages over 30 seconds.

284

285 *b) Meteorological observations and calculations*

286 Standard meteorological parameters, including altitude, ambient temperature (T), wind speed
287 (U), wind direction (WD), air pressure (p), and relative humidity (RH), were measured for the
288 elevated-altitude samples using a standard meteorology package positioned approximately
289 20 m below the balloon (Pilz et al., 2023). The potential temperature (θ) within the
290 atmospheric column - as a measure of the static stability of the unsaturated atmosphere - was
291 calculated using Eq. I, where T is the ambient temperature (K), p is the atmospheric pressure
292 (hPa), p_0 is the reference pressure (1000 hPa), R is the specific gas constant ($287 \text{ J kg}^{-1} \text{ K}^{-1}$) and
293 c_p is the specific heat capacity of dry air at constant pressure ($1004 \text{ J kg}^{-1} \text{ K}^{-1}$).

294
$$\theta = T \left(\frac{p_0}{p} \right)^{\frac{R}{c_p}} \quad (\text{Eq. I})$$

295 Specific humidity (q)–remaining constant during adiabatic ascent or descent as long as no
296 phase changes occur–was calculated using Eq. II from Egerer et al. (2021), where R_d/R_v (the
297 ratio of specific gas constants for dry air and water vapor) is approximately 0.622, and $e_s(T)$
298 represents the temperature-dependent saturation vapor pressure.

299
$$q = \frac{R_d/R_v \cdot e_s(T) \cdot RH}{p - (1 - R_d/R_v) \cdot e_s(T) \cdot RH} \quad (\text{Eq. II})$$

300 Meteorological data measured 2 m above the ground (13 m above sea level) at the AWIPEV
301 Atmospheric Observatory (Maturilli, 2020), represented the weather conditions during
302 aerosol sampling at the winch.

303 **2.5 Supporting observations and model calculations**

304 Major inorganic ions measured at the Zeppelin Observatory with 24-hour resolution using a
305 stationary aerosol sampler (Filter_3pack) were obtained from the EBAS database (Aas et al.,
306 2022, 2023) for the study period. The measurements are part of the European Monitoring and
307 Evaluation Programme (Tørseth et al., 2012) and were conducted by the Norwegian Polar
308 Institute (NPI) and the Norwegian Institute for Air Research (NILU). The Filter_3pack data were
309 utilized in two ways:

- 310 1. **Comparing sampling techniques:** Data from the Filter_3pack were compared with one
311 HALFBAC aerosol particle sample collected directly at the Zeppelin Observatory (Filter
312 ID 62, 10 May 2022) to evaluate potential artifacts arising from differences in sampling
313 techniques and filter media. Despite variations in time resolution and methods,
314 sodium, potassium, chloride, and sulfate concentrations showed strong agreement
315 (detailed in the supplement A2 and **Figure S2**).
- 316 2. **Comparison with balloon data:** Sodium concentrations measured at the Zeppelin
317 Observatory were directly compared with those obtained from the tethered balloon
318 sampling.

319 Information on the occurrence of clouds and hydrometeor types at Ny-Ålesund were taken
320 from the Cloudnet classification product (Illingworth et al., 2007; Nomokonova et al., 2019),
321 which is based on a combination of ground-based cloud radar, ceilometer, and numerical
322 weather prediction output. Vertically integrated ice water content (IWC), i.e. ice water path
323 (IWP), has been calculated from the Cloudnet IWC product following Hogan et al. (2006).
324 Vertically integrated cloud liquid water (liquid water path; LWP) and water vapor (IWV) were
325 taken from zenith HATPRO microwave radiometer measurements (Nomokonova et al., 2019).

326 The 48-hour back-trajectories for the aerosol sampling periods were generated using the
327 NOAA HYSPLIT model (Stein et al., 2015). Trajectories were calculated hourly based on GDAS1
328 meteorological data (Global Data Assimilation System; 1° spatial resolution; 3-hour intervals)
329 for various arrival heights: 50 m (ground level), 474 m (Zeppelin Observatory), and the specific
330 balloon sampling altitudes. Sea ice concentration data were obtained from the NOAA-
331 maintained ERDDAP server (Environmental Research Division's Data Access Program). The
332 back-trajectories were used to assess the relative influence of distant sources, such as the
333 marginal ice zone, versus local ice-free oceanic emissions on the aerosol chemical

334 composition. Given the rather short atmospheric residence time of supermicron SSA particles
335 (Madry et al., 2011; Veron, 2015), which account for most of the SSA mass in TSP, and the
336 increasing uncertainties associated with longer back-trajectory periods, we considered a 48-
337 hour back-trajectory length appropriate for this analysis.

338 Ocean surface concentrations for total chlorophyll *a* (TChl-*a*) and dissolved acidic
339 polysaccharides were obtained by a coupled setup of the ocean sea ice biogeochemistry
340 model FESOM2.1-REcoM3 (Gürses et al., 2023), to which additional state equations have been
341 added to simulate dissolved and particulate organic carbon following Engel et al. (2004) and
342 Schartau et al. (2007). The simulation was set up following Gürses et al. (2023) and using the
343 Arctic-specific tuning of Oziel et al. (2022). The modelled dissolved acidic polysaccharides were
344 used as a proxy for dCCHO. Although they represent only a fraction of dCCHO, their
345 concentrations were shown to be within the same order of magnitude as field observations
346 (Zeising et al., 2026). Monthly model output was obtained on an irregular grid with
347 approximately 4.5 km resolution in the Arctic Ocean. This configuration has already been
348 applied successfully in Leon-Marcos et al. (2025).

349

350 **2.6 Statistics, data processing, visualization and text optimization**

351 Statistical analyses, calculations and visualization were conducted using OriginPro 2024,
352 Microsoft Excel, IDL, python3 and R version 4.2.1 with the ncd4 (Pierce, 2023), openair
353 (Carslaw and Ropkins, 2012), reshape2 (Wickham, 2007), scales (Wickham et al., 2023b),
354 lubridate (Grolemund and Wickham, 2011), cmocean (Thyng et al., 2016), maps (Brownrigg,
355 2023), mapdata (Brownrigg, 2013), rgdal (Bivand et al., 2022), raster (Hijmans, 2023),
356 RColorBrewer (Neuwirth, 2022), sp (Bivand et al., 2013), dplyr (Wickham et al., 2023a), ggplot2
357 (Wickham, 2016), and PlotSvalbard (Vihtakari, 2020) packages. Box-and-whisker plots
358 illustrate the interquartile range (box), the median (horizontal line inside the box), the mean
359 (open square), the minimum and maximum values (whiskers). Text and language were
360 optimized using Open AI's ChatGPT-4 Turbo.

361 **3. Results and Discussion**

362 **3.1 Chemical constituents in marine aerosol particles from their oceanic source** 363 **to elevated altitudes**

364 ***Sodium in aerosol particles (Na^+_{aer})***

365 Sodium, a dominant and chemically stable component of SSA, is commonly used as a tracer
366 for tracking ocean-derived emissions in atmospheric studies (Manders et al., 2010; van
367 Pinxteren et al., 2017; White, 2008). In this study, consistently high Na^+_{aer} concentrations were
368 observed on the TSP filters at the Old Pier next to Kongsfjorden in both autumn 2021 and
369 spring 2022 (**Figure 2a**), ranging from 140 to 1470 ng m^{-3} (median: 495 ng m^{-3} ; $n=8$). The area
370 around Ny-Ålesund, especially the Old Pier, remained largely ice-free, indicating a negligible
371 influence of local sea ice on SSA emissions.

372 Na^+_{aer} at the winch site, located further inland but still at ground level (35–3710 ng m^{-3} ;
373 median: 155 ng m^{-3} ; $n=17$), and at the balloon (321–1112 m; 23–850 ng m^{-3} ; median:
374 124 ng m^{-3} ; $n=15$) was generally lower than at the Old Pier, though episodic high events
375 occurred at all sites. This wide variability from low ng m^{-3} to a few $\mu\text{g m}^{-3}$ agrees with
376 observations from other marine environments and altitudes (Fomba et al., 2014; Li et al.,
377 2024; Ooki et al., 2002; Theodosi et al., 2010; Triesch et al., 2021; Zeppenfeld et al., 2021,
378 2023).

379 Since winch and balloon sampling were always synchronized, direct comparisons were
380 possible (**Figure 3**). Several events showed nearly identical Na^+_{aer} concentrations (winch vs.
381 balloon), e.g., 30 Sep: 191 vs. 207 ng m^{-3} ; 2 Oct: 35 vs. 36 ng m^{-3} ; 9 Oct: 59 vs. 60 ng m^{-3} ; 12
382 Nov: 240 vs. 223 ng m^{-3} . In contrast, other periods exhibited strong vertical gradients with
383 higher ground-level concentrations (e.g., 27 Sep: 1840 vs. 23 ng m^{-3} ; 5 Apr: 84 vs. 54 ng m^{-3} ;
384 11 May: 496 vs. 125 ng m^{-3}), while two cases showed higher values at the balloon (24 Sep: 47
385 vs. 99 ng m^{-3} ; 3 Apr: 77 vs. 194 ng m^{-3}). These variations are likely driven by atmospheric
386 processes, including dry and wet deposition (Farmer et al., 2021), dilution during vertical and
387 horizontal transport from the emission region (Wong et al., 2019), vertical mixing (Pilz et al.,
388 2024) and differing air mass histories (Willis et al., 2018), which will be examined in detail for
389 three selected cases later in this study.

390 Na^+_{aer} at the Zeppelin Observatory largely agreed with the balloon measurements (56–213%
 391 overall; 92–107% in five events; **Table S6**), despite differences in time resolution (24 h vs. 1–
 392 2 h), sampling altitude, the horizontal distance between the sites, Svalbard’s complex
 393 topography (Gierens et al., 2020; Shestakova et al., 2021), and the fact that meteorological
 394 conditions and atmospheric mixing states have not yet been considered.

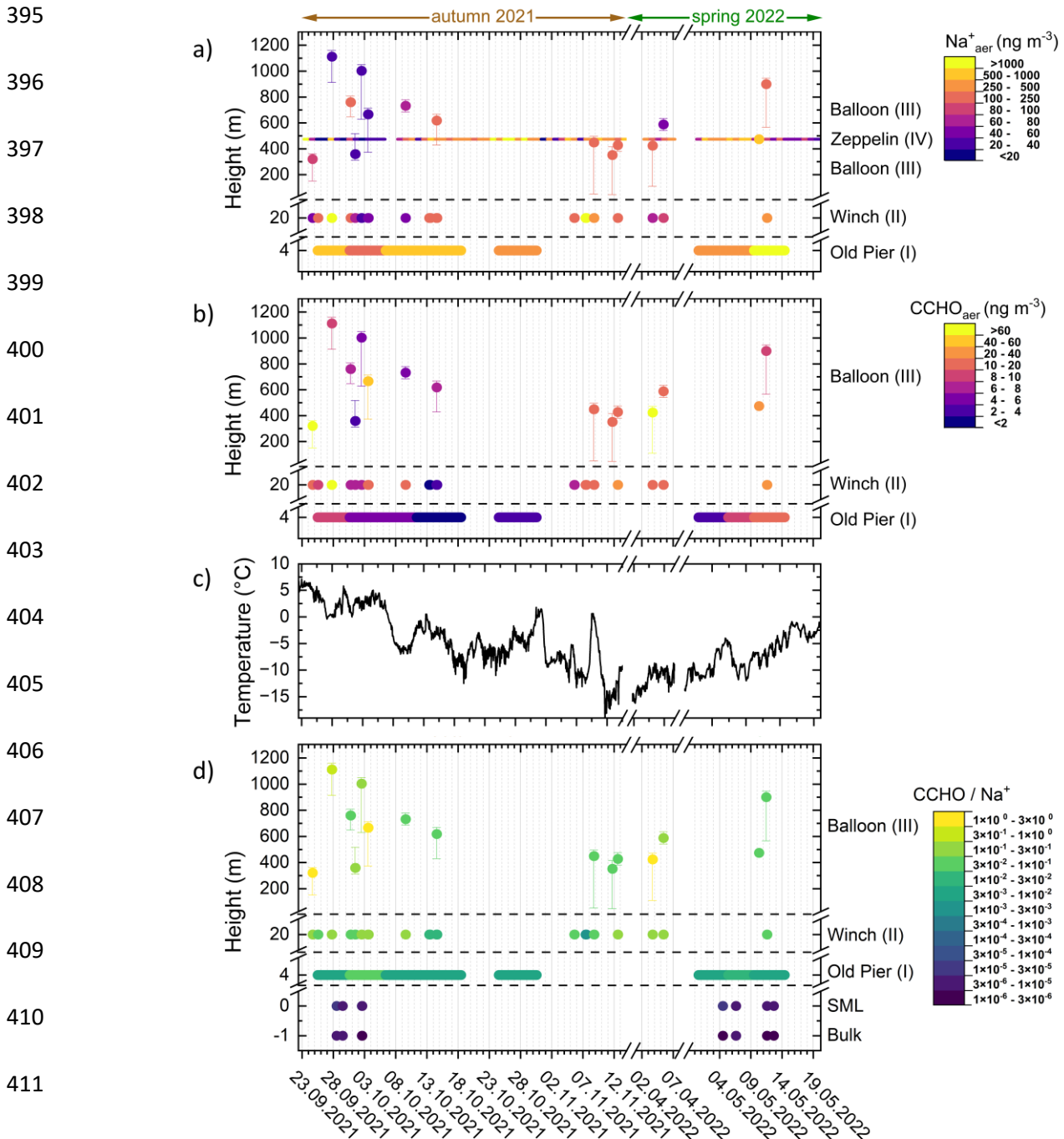


Figure 2. Time-resolved atmospheric concentrations of a) Na^+_{aer} and b) CCHO_{aer} in aerosol particles (TSP) collected in autumn 2021 and spring 2022 in Ny-Ålesund at several heights (m a.s.l.) from four sites: Old Pier, winch near the AWIPEV Observatory, balloon and the Zeppelin Observatory. Dots represent the median height during the total sampling time and vertical error bars represent maximum and minimum height of the sampler during the active sampling. The x-axis ticks represent the start of each date at midnight. c) Air temperature (2 m above ground) measured at the AWIPEV Observatory. d) CCHO/Na^+ ratios within the bulk seawater, the SML and in the aerosol particles at several heights. In panel (a), the label “Balloon (III)” appears twice because balloon sampling for sodium measurements occurred both below and above the fixed altitude of the Zeppelin Observatory.

415 Overall, Na^+_{aer} was detectable up to 1100 m altitude, sometimes at levels comparable to those
 416 near the emission source, indicating effective vertical mixing or transport to cloud-relevant
 417 heights via advection. This vertical distribution is consistent with the aircraft-based SSA
 418 measurements reported by Hara et al. (2003) and Köllner et al. (2017). Longer atmospheric
 419 residence increases the exposure of SSA particles to processing, which can alter their impact
 420 on cloud formation. While Na^+_{aer} is considered chemically stable, co-emitted OM including
 421 carbohydrates may undergo physical, chemical and microbial changes (Zeppenfeld et al.,
 422 2021, 2023). This aspect will be explored further in section 3.3.

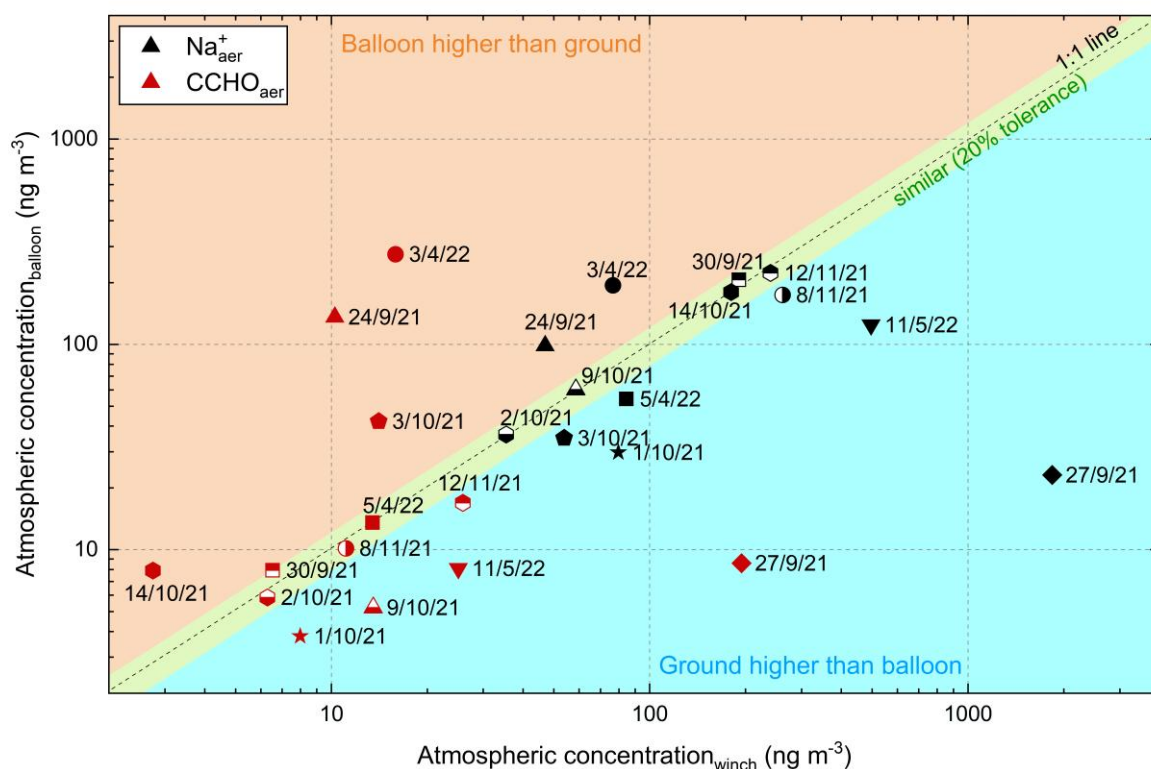


Figure 3. Scatter plot showing Na^+_{aer} (black symbols) and CCHO_{aer} (red symbols) concentrations in TSP measured at the winch, and balloon levels. Marker shapes and fill styles serve as identifiers linking corresponding Na^+_{aer} and CCHO_{aer} values from the same sample. Data points are categorized to indicate whether values were similar, higher at the balloon, or higher at the ground.

423
 424
 425
 426

427 ***Combined carbohydrates in fresh SSA and surface seawater***

428 Similar to sodium, CCHO_{aer} were detected at all sites and altitudes (**Figure 2b**). At the Old Pier,
429 CCHO_{aer} concentrations ranged from 1.6 to 10.0 ng m⁻³ (median: 5.0 ng m⁻³; n=8), showing a
430 seasonal pattern with the highest values at the beginning (end of September 2021) and end
431 (mid of May 2022) of the study period, and lower values in October 2021, coinciding with low
432 air temperatures (**Figure 2c**). No samples were collected between November and April, so
433 winter trends remain unknown.

434 A seasonal trend was also observed for dCCHO in Kongsfjorden seawater. Concentrations
435 peaked in late September/early October and were substantially lower in early to mid-May,
436 averaging only about 50% of the autumn values (**Figure 4**). Most monosaccharides in bulk
437 dCCHO showed a strong co-variation with SST ($R^2= 0.79-0.93$; n = 11). This relationship was
438 weaker for xylose ($R^2_{\text{Xyl-SST}} = 0.62$) and glucose ($R^2_{\text{Glc-SST}} = 0.53$) in bulk dCCHO, and generally
439 more moderate in the SML for most monosaccharides (**Figure 4**).

440 In contrast, pCCHO as a whole showed no clear seasonal trend in seawater (**Figure S3**).
441 However, a few monosaccharides within bulk water pCCHO, in particular fucose, glucosamine,
442 and galactosamine, displayed a moderate correlation with SST ($R^2_{\text{Fuc-SST}} = 0.73$; $R^2_{\text{GalN-SST}} =$
443 0.39 ; $R^2_{\text{GlcN-SST}} = 0.69$; n=11). While dCCHO in bulk water exhibited relatively low spatial and
444 intra-seasonal variability, pCCHO and SML samples were considerably more variable, even
445 among samples from the same season (**Figure S4**). This likely reflects the rapid dynamics of
446 pCCHO in relation to phytoplankton blooms (Becker et al., 2020; Engel et al., 2012; Fabiano et
447 al., 1993), as well as the formation of transparent exopolymer particles (TEP) from dCCHO in
448 turbulent waters and vertical transport of pCCHO via sedimentation (e.g., as marine snow) or
449 its accumulation in the SML depending on buoyancy (Burns et al., 2019; Engel, 2004; Robinson
450 et al., 2019a, b; Wurl and Holmes, 2008). The SML, in particular, may be more sensitive to
451 these dynamics than the bulk water, potentially explaining its greater fluctuations.

452

453

454

455

456

457

458

459

460

461

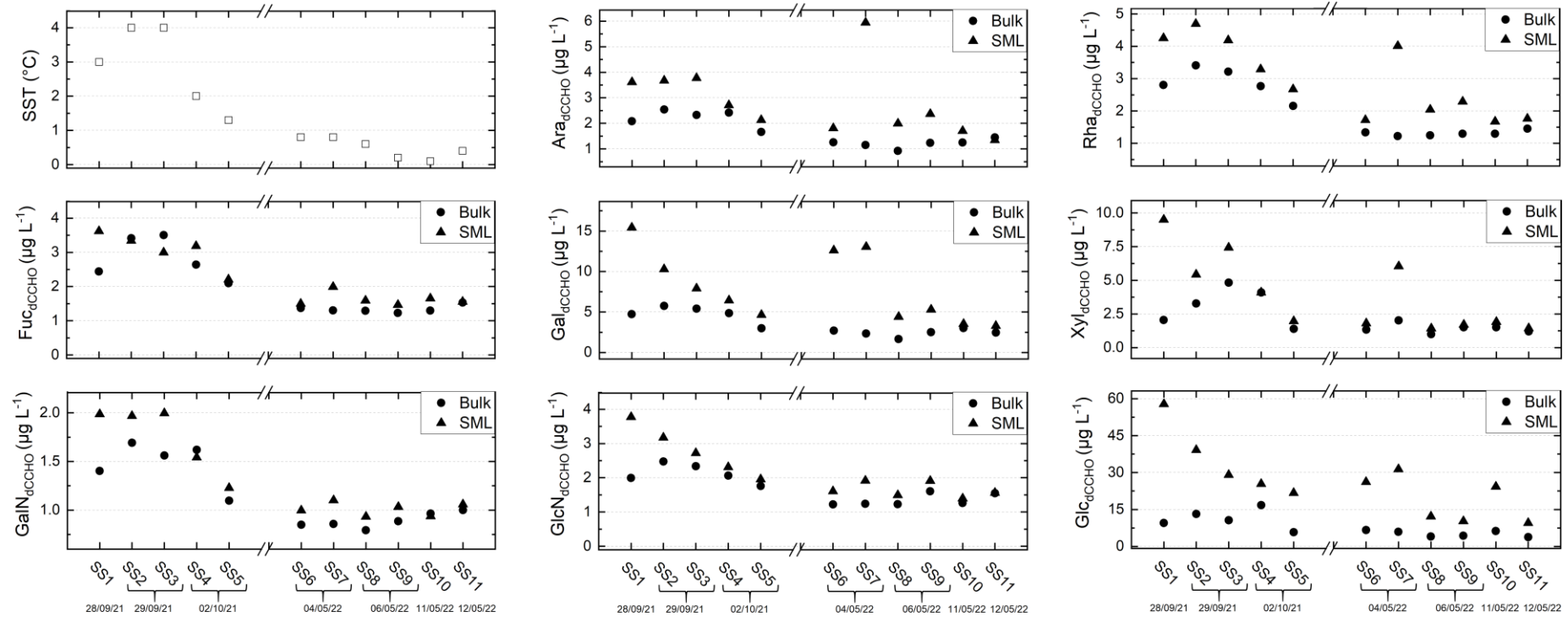


Figure 4. Concentration of measured monosaccharide units in dCCHO from bulk and SML samples collected in Kongsfjorden during autumn 2021 and spring 2022, along with SST measurements taken from bulk samples at the time of sampling.

462 By comparison, dCCHO in bulk water, like dissolved organic carbon (Hansell, 2013; Keene et
463 al., 2017), is likely dominated by recalcitrant and semi-recalcitrant compounds, while the labile
464 fraction is rapidly consumed by heterotrophic bacteria (Goldberg et al., 2011). Notably,
465 combined glucose showed high variability in both dCCHO and pCCHO, likely due to being the
466 main constituent of abundant storage macromolecules such as laminarin (Becker et al., 2020),
467 whose production and turnover may be enhanced during periods of photosynthetic overflow
468 (Barthelmeß et al., 2025), as well as its relatively rapid microbial utilization (Kharbush et al.,
469 2020).

470 The seasonal variation of CCHO_{aer} at the Old Pier may be linked to the seasonal dynamics of
471 marine CCHO in the surface waters of Kongsfjorden, the only local emission source of SSA.
472 These dynamics are likely driven by seasonal shifts in primary production and phytoplankton
473 composition (Assmy et al., 2023; Mayot et al., 2018, van de Poll et al., 2021).

474 Overall, CCHO_{aer} and selected seawater dCCHO monosaccharides showed a broadly consistent
475 seasonal tendency, with elevated values in late summer/early autumn. However, the spring
476 conditions (May) deviate from this pattern, with CCHO_{aer} showing a secondary maximum that
477 is not reflected in seawater dCCHO, where concentrations remain substantially lower. This
478 indicates that the seasonal coupling between (bulk) seawater CCHO and CCHO_{aer} is strongest
479 in late summer/early autumn, while additional processes such as SML enrichment or
480 atmospheric processing may also contribute to the spring aerosol signal.

481 In conclusion, the seasonal variation of CCHO_{aer} measured at the Old Pier is partly consistent
482 with marine carbohydrates in Kongsfjorden seawater, suggesting that surface CCHO is an
483 important but not exclusive source of freshly emitted CCHO_{aer}.

484 ***CCHO_{aer} at the winch and higher altitudes***

485 CCHO_{aer} at the winch site (1.9–194 ng m⁻³; median: 10.6 ng m⁻³; n=17) and at the balloon (3.8–
486 274 ng m⁻³; median: 10.2 ng m⁻³; n=15), showed broader ranges and significantly higher
487 median and maximum values than at the Old Pier (**Figure 2b**), suggesting sources beyond
488 primary sea-air transfer. No clear seasonal pattern (in contrast to the Old Pier) or altitude
489 dependence was observed, likely due to the winch site's inland location, making it more
490 sensitive to wind direction and changing weather. Also, the higher temporal resolution of the

491 samples likely captured short-term fluctuations rather than integrated seasonal trends. In
492 addition, atmospheric processing during transport and the lack of true winter samples may
493 have further obscured any clear seasonal signal.

494 Similar to sodium, some events (**Figure 3**) showed comparable CCHO_{aer} at the winch and
495 balloon (e.g., 30 Sep: 6.5 vs. 8.0 ng m⁻³; 2 Oct: 6.3 vs. 5.8 ng m⁻³; 8 Nov: 11.1 vs. 10.2 ng m⁻³),
496 while on other dates, concentrations were markedly lower at higher altitudes (e.g., 27 Sep:
497 194 vs. 8.6 ng m⁻³; 11 May: 25 vs. 8.1 ng m⁻³), or conversely, higher aloft (e.g., 24 Sep: 10.2 vs.
498 136 ng m⁻³; 3 Apr: 15.9 vs. 275 ng m⁻³). In most cases, CCHO_{aer} covaried with sodium except on
499 03 Oct, when Na⁺_{aer} was slightly higher at the ground (54 vs. 35 ng m⁻³), whereas CCHO_{aer} was
500 higher at the balloon (42 ng m⁻³) than at the winch (14 ng m⁻³).

501 To investigate oceanic emission and the atmospheric fate of marine CCHO, CCHO/Na⁺ ratios
502 were calculated for all aerosol, bulk seawater and SML samples, representing the primary
503 sources of the SSA particle constituents studied here (**Figure 2d**). Bulk seawater showed the
504 lowest ratios (2.0×10^{-6} – 6.0×10^{-6}) with minimal variability, while the SML had slightly higher
505 ratios (3.3×10^{-6} – 2.5×10^{-5}) due to CCHO enrichment. Specifically, the enrichment factors
506 (EF_{SML}) ranged 1.3 – 4.1 for dCCHO and 0.9 – 6.8 for pCCHO (**Figure S4**), which aligns well with
507 previous studies (Engel and Galgani, 2016; Gao et al., 2012; Zäncker et al., 2021; Zeppenfeld
508 et al., 2021, 2023).

509 At the Old Pier, where fresh SSA was sampled, the ratios were significantly higher (6.2×10^{-3}
510 – 3.3×10^{-2}) indicating the chemo-selective sea-air transfer that enriches surface-active
511 organics relative to sodium in aerosol particles (Hasenecz et al., 2020, 2019; Jayarathne et al.,
512 2016; Schill et al., 2018; Zeppenfeld et al., 2021, 2023). The enrichment effect is typically more
513 pronounced in submicron particles, which have a higher relative contribution of organics than
514 inorganic ions (Quinn et al., 2015). In contrast, supermicron particles are predominantly
515 composed of sea salts, although organic substances are still notably enriched compared to the
516 surface seawater. As total suspended particles were measured here, and most SSA mass
517 resides in the supermicron range (Facchini et al., 2008; O'Dowd et al., 1997), our results
518 primarily reflect supermicron aerosol composition.

519 At the winch sampling station, located at ground level but further inland, the CCHO/Na⁺ ratios
520 in TSP ranged from 2.9×10^{-3} to 2.6×10^{-1} , similar or slightly higher than at the Old Pier. In
521 contrast, balloon samples from elevated altitudes showed higher ratios (3.9×10^{-2} – 1.4×10^0),

522 likely due to depletion of salt-rich supermicron particles during dry and wet deposition (Croft
523 et al., 2009; Hoppel et al., 2002; O'Dowd and de Leeuw, 2007), increasing the relative
524 contribution of OM-dominated submicron particles. Furthermore, the increasing absolute
525 concentration of CCHO at higher altitudes (**Figure 2b**) suggests an atmospheric formation
526 process contributing to the elevated CCHO/Na⁺ ratios, potentially linked to microbial activity
527 in the atmosphere (see section 3.3). However, because only the major monosaccharides
528 (typically Glc, Xyl, Gal, Ara) could be quantified reliably in the winch and balloon samples,
529 relative CCHO compositions were not assessed across the entire vertical sample set.
530 Therefore, they were not used to further substantiate this conclusion, as it has been done in
531 Zeppenfeld et al. (2021, 2023).

532 The CCHO/Na⁺ ratios observed at the Old Pier and the Winch closely align with ship-based
533 measurements from the PASCAL cruise (May–July 2017) in the Fram Strait, Barents Sea, and
534 central Arctic Ocean (Macke and Flores, 2018; Wendisch et al., 2018), where values ranged
535 from 2×10^{-3} to 2×10^{-1} in PM₁₀ based on summed Berner impactor stages (Zeppenfeld et al.,
536 2023). In contrast, the very high CCHO/Na⁺ values ($>1 \times 10^0$) observed at some elevated
537 altitudes in this study were reported only occasionally for submicron particles (0.14–0.42 μm)
538 during PASCAL. This may support the idea that supermicron particle deposition caused the
539 shift in balloon sample ratios, though microbial contributions in the atmosphere are also
540 possible. Moreover, these ratios far exceed those from the Southern Ocean near the western
541 Antarctic Peninsula (8×10^{-4} to 7×10^{-3}) (Zeppenfeld et al., 2021), likely due to differences in
542 surface seawater productivity.

543 Overall, it can be concluded that both Na⁺_{aer} and CCHO_{aer} are transported from the marine
544 emission source to elevated heights within the lower troposphere. In the following section,
545 we discuss the role of meteorological conditions and atmospheric mixing in linking ground-
546 based and balloon-based samples.

547 **3.2 Impact of meteorological conditions on SSA particle constituents in higher**
 548 **altitudes**

549 To examine how meteorological conditions and atmospheric mixing influence Na^+_{aer} and
 550 CCHO_{aer} at high altitudes, three distinct cases with constant weather conditions were selected
 551 (**Figure 5**). These conditions allow for a detailed interpretation of the observed chemical
 552 values.

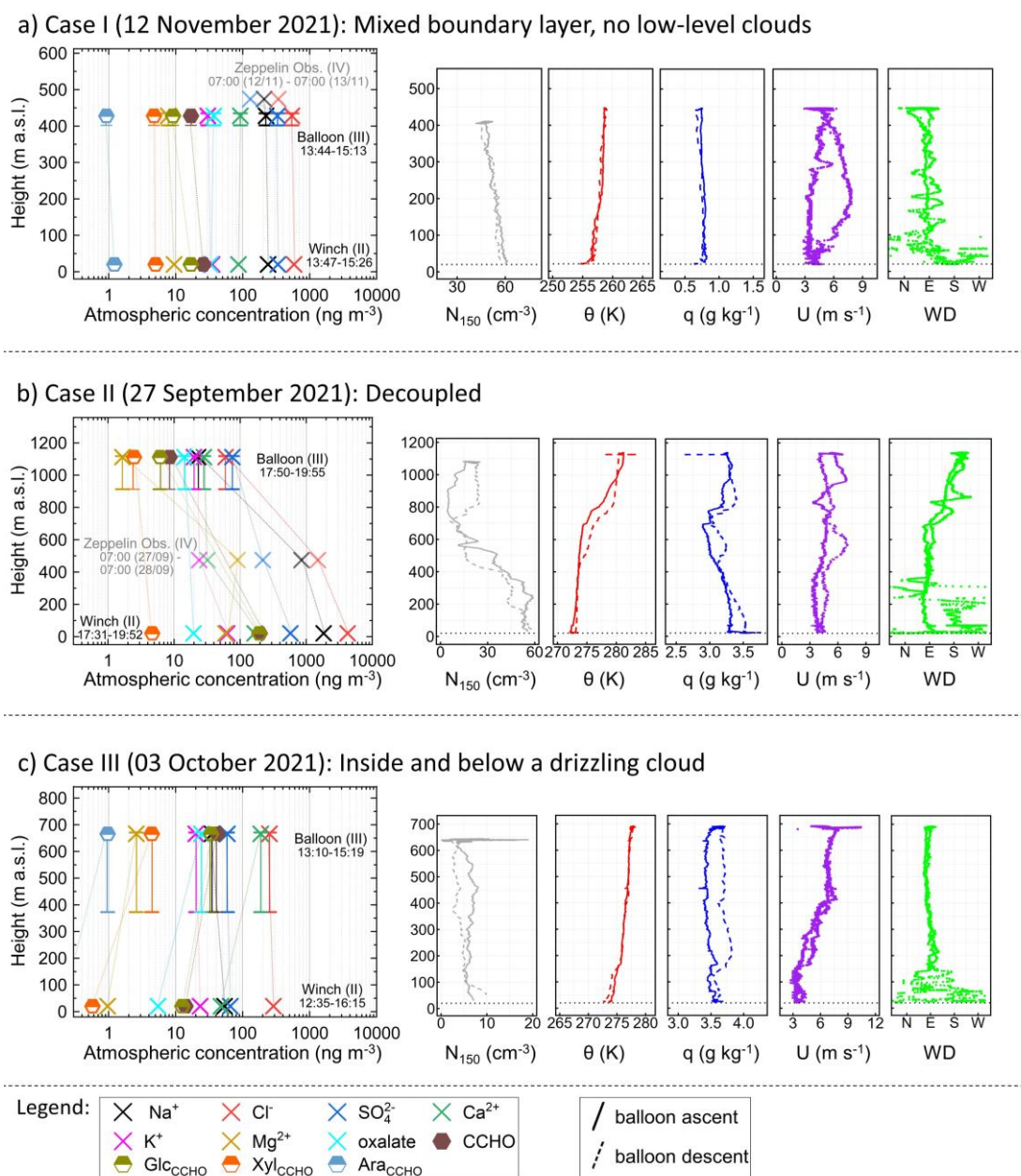


Figure 5. Vertical profiles of three atmospheric cases showing mass concentrations of chemical constituents (inorganic ions, oxalate, total CCHO_{aer} , and major monosaccharides within CCHO_{aer}) in aerosol particles, measured on the ground (winch) and aloft (balloon) using offline filters. Vertical error bars indicate the range between minimal and maximal heights during active sampling at the balloon, while the symbols denote the median sampling heights. Data from the Zeppelin Observatory are also included when available and above detection limits, albeit with a 24-hour resolution. Dotted lines are included to aid in reading the vertical distribution of individual chemical substances. These profiles are complemented by aerosol particle number concentrations of particles bigger than 150 nm (N_{150}), potential temperature (θ), specific humidity (q), wind speed (U), and wind direction (WD) measured during the ascents (solid lines) and descents (dashed lines) of the balloon.

553 To assess atmospheric stability and layering in these cases, vertical profiles of potential
 554 temperature were utilized. To further confirm aerosol mixing conditions, additional
 555 meteorological parameters (specific humidity, wind speed and direction), vertical aerosol
 556 particle number concentrations of particles larger than 150 nm (N_{150}) (**Figure 5**), cloud
 557 conditions (**Figure S5**) and back-trajectory analyses (**Figure 6**) were considered. The selected
 558 cases include (a) a cloud-free mixed boundary layer (12 Nov 2021), (b) a free troposphere
 559 decoupled from the ground (27 Sep 2021), and (c) a boundary layer capped by precipitating
 560 clouds (03 Oct 2021).

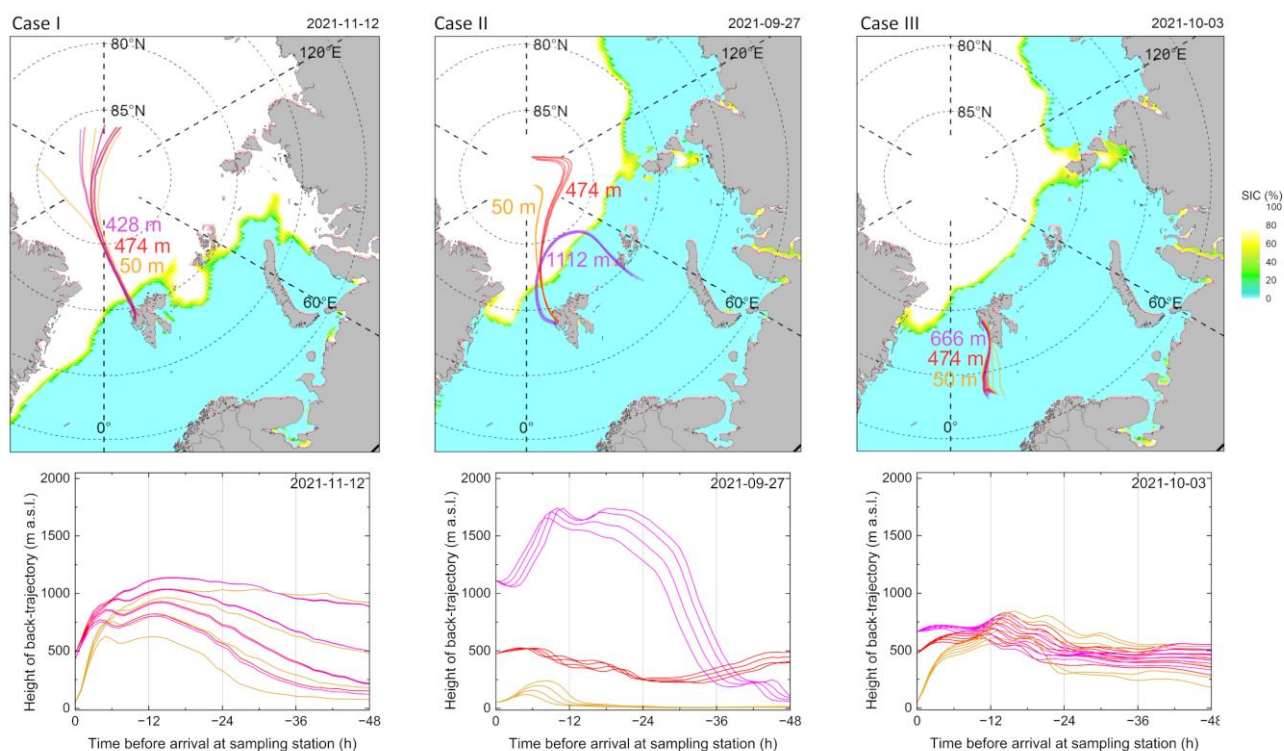


Figure 6. 48-hour back-trajectories calculated on an hourly basis for three arrival heights: orange (50 m, ground-level air masses), red (474 m, height of the Zeppelin Observatory), and purple (variable arrival height, high-altitude air masses sampled at tethered balloon). These are accompanied by daily sea ice concentration (SIC) maps (top) and height profiles (bottom) for three selected aerosol particle sampling cases.

561 **Case I: Mixed boundary layer & no low-level clouds**

562 On 12 November 2021, during the polar night, two HALFBACs were operated simultaneously
 563 at the ground and the balloon (median altitude of 428 m) for approximately 90 min. Ground-
 564 level conditions were -16.7°C , 69% RH, and 1.5 m s^{-1} wind mainly from the southwest. At the
 565 balloon, sampling occurred at a similar temperature (-17.5°C) and RH (72%), but higher wind
 566 speeds (4.3 m s^{-1}) from the northeast to southeast. With $\text{IWV} < 3\text{ kg m}^{-2}$, the atmosphere was
 567 very dry (**Figure S5a**), and only a thin mixed-phase cloud layer at 4.5–5 km altitude was

568 present, with negligible LWP and IWP (**Figure S5a**), unlikely to affect aerosol chemistry within
569 the boundary layer.

570 During the balloon's ascent, potential temperature increased from 255 K to 258 K, with the
571 strongest gradient near the ground. Using the wind speed profile and the Richardson number
572 approach (Akansu et al., 2023), a very shallow surface mixing layer of ~12 m was estimated,
573 likely caused by recent surface cooling. Although this surface inversion and the slightly stable
574 to near-neutral stratification above would limit instantaneous vertical mixing, surface mixing
575 layer height reflects only momentary conditions, whereas aerosol and humidity profiles
576 integrate mixing over longer timescales. The coupling state at the time of measurement is
577 therefore not a reliable indicator of the effective boundary-layer mixing state. Furthermore,
578 as noted in Section 2.1, Ny-Ålesund's complex orography can induce localized turbulent mixing
579 even under stable stratification. In addition, a low-level jet observed during descent, with wind
580 speeds at least 2 m s⁻¹ higher than above and below, provided a significant additional source
581 of turbulence and vertical mixing within the boundary layer (Egerer et al., 2023).

582 At the ground, N₁₅₀ was around 60 cm⁻³, and gradually decreased to 45 cm⁻³ at the balloon's
583 sampling height, indicating a fairly uniform aerosol distribution dominated by primary
584 emissions. Combined with nearly constant specific humidity (~0.7–0.8 g kg⁻¹), a slight wind
585 speed increase with altitude, the low-level jet during descent, and consistent wind direction
586 (**Figure 4a**), these suggest a largely well-mixed boundary layer. HALFBAC samples from ground
587 and balloon showed similar concentrations of inorganic ions (Na⁺_{aer}: 240 & 223, Cl⁻_{aer}: 586 &
588 543, SO₄²⁻_{aer}: 336 & 330, Ca²⁺_{aer}: 87 & 92, Mg²⁺_{aer}: 9.5 & 7.8, K⁺_{aer}: 34 & 30 ng m⁻³), oxalate_{aer}
589 (34 & 37 ng m⁻³), and major CCHO-bound monosaccharides (Glc_{CCHO,aer}: 17 & 9.1, Xyl_{CCHO,aer}:
590 5.0 & 4.7, Ara_{CCHO,aer}: 1.2 & 0.9 ng m⁻³), supporting a well-mixed layer. Despite diverse sources
591 (SSA, dust, anthropogenic, secondary), vertical aerosol composition remained uniform.
592 Zeppelin Observatory 24 h measurements of Na⁺_{aer}, Cl⁻_{aer}, and SO₄²⁻ showed slightly lower
593 concentrations but agreed with balloon results.

594 Back-trajectory analysis revealed that air masses at ground level, the balloon, and Zeppelin
595 Observatory (**Figure 6, Case I**) followed the same path during the 48 hours before sampling.
596 Originating from the Arctic pack ice, they crossed the marginal ice zone with a short residence
597 time before passing over the ice-free ocean and Kongsfjorden, where most SSA compounds
598 were likely taken up. The back-trajectory heights indicate a vertical connection between the

599 three air masses, confirming a similar transport history, influenced by the same emission
600 sources.

601 This case demonstrates that major SSA constituents (Na^+_{aer} , Cl^-_{aer} , and CCHO_{aer}) can mix
602 effectively within the boundary layer, reaching altitudes relevant to cloud formation with
603 concentrations nearly identical to ground level, and that such a mixing state can persist during
604 temporarily decoupled conditions, provided there is no additional aerosol particle source at
605 the ground or aloft.

606 ***Case II: Free troposphere decoupled from the ground***

607 On 27 September 2021, balloon measurements were conducted at a median altitude of
608 1112 m, above both the Zeppelin Observatory and the altitude range of Case I, i.e. in the free
609 troposphere above the boundary layer. A strong increase of the potential temperature
610 between 700 m ($\theta \approx 274$ K) and 900 m ($\theta \approx 280$ K) indicates a pronounced inversion (**Figure 5b**).
611 N_{150} peaked near the ground, remained stable in the lowest 200 m, decreased up to ~ 700 m,
612 and slightly increased toward 1112 m, suggesting sources other than the ground. Specific
613 humidity varied strongly (2.6–4 g kg⁻¹), confirming a decoupled atmospheric layer.

614 During ground sampling, mean conditions were 3 °C, 89 % RH, and 0.7 m s⁻¹ wind from the
615 southwest (**Table S5**). At balloon altitude, air was colder (–1.9 °C), slightly drier (87 % RH), and
616 much windier (5.5 m s⁻¹), primarily from the south and southwest (**Table S4**). IWV increased
617 from 13 to ~ 15 kg m⁻² during sampling (**Figure S5b**). A dense warm-front cloud layer (2–8 km)
618 with mainly cloud ice (IWP up to 1.4 kg m⁻²) was present (**Figure S5b**). Precipitation reached
619 the balloon as snowfall only in the last 15–30 min of sampling.

620 On this date, we observed a strong vertical gradient in both Na^+_{aer} and CCHO_{aer} concentrations
621 (**Figure 5b**), starting from the winch (Na^+_{aer} : 1840 ng m⁻³, CCHO_{aer} : 199 ng m⁻³), decreasing at
622 the Zeppelin Observatory (Na^+_{aer} : 850 ng m⁻³), and dropping sharply at the balloon's altitude
623 (Na^+_{aer} : 23 ng m⁻³, CCHO_{aer} : 8.6 ng m⁻³). Similar declines occurred for $\text{SO}^{2-}_{4\text{aer}}$ (580; 220;
624 76 ng m⁻³), Cl^-_{aer} (4230; 1500; 60 ng m⁻³), and $\text{Ca}^{2+}_{\text{aer}}$ (165; 32; 28 ng m⁻³). This pronounced
625 decrease with altitude indicates separation between ground-level and elevated air masses,
626 making fresh local SSA from Kongsfjorden or the west coast of Svalbard an unlikely source for
627 the substances detected at 1112 m.

628 This assumption is supported by back-trajectory analysis (**Figure 6b**): air masses at 50 m and
629 474 m arrival height originated from Arctic pack ice and crossed the ice-free Fram Strait,
630 whereas the 1112 m air mass followed a different path over the Barents Sea near Franz Josef
631 Land. After contact with the marine boundary layer and possibly the sea surface about 48 h
632 before sampling, it remained mainly between 1000 and 1800 m. This indicates that the SSA
633 observed at 1112 m in Ny-Ålesund likely originated from this distant source region.

634 In summary, Case II demonstrates that major SSA constituents (Na_{aer}^+ , $\text{Ca}_{\text{aer}}^{2+}$, Cl_{aer}^- , $\text{SO}_{4\text{ aer}}^{2-}$
635 and CCHO_{aer}) can be present in the free troposphere and likely originate from a distant source.
636 However, they appear at lower concentrations above the inversion than in the boundary layer
637 below, where concentrations, as in Case I, are more similar to those at the ground.

638 ***Case III: Inside and below a drizzling cloud***

639 On 03 October 2021, the ground temperature was 3°C with a high relative humidity of 89%.
640 Winds were light, shifting between east, south, and west at 0.7 m s⁻¹ during sampling. At the
641 balloon's altitude of 666 m, the average temperature was -1.3°C, the relative humidity 96%
642 and the wind speed 6.8 m s⁻¹ from the east and northeast. The day was overcast, with
643 continuous drizzle from a 2 km deep mixed-phase cloud layer with LWP values of up to
644 300 g m⁻² and IWV of around 13 to 14 kg m⁻². The balloon's altitude was close to the melting
645 layer.

646 During the balloon's ascent and descent to 666 m, a positive gradient in potential temperature
647 (272 K at the ground vs. 278 K at the balloon, **Figure 5c**) indicated a stably stratified boundary
648 layer. Specific humidity was uniform (3.2–3.8 g kg⁻¹), while N_{150} was lower than in Case I (3–10
649 cm⁻³) with higher relative variability, likely influenced by low counting statistics at these low
650 concentrations. Overall, mixing conditions in Case III were similar to Case I, but sampling
651 occurred partly within or below a drizzling low-level cloud.

652 Back-trajectory analysis (**Figure 6, Case III**) showed that air masses at the altitudes of ground,
653 balloon, and Zeppelin Observatory followed the same 48-h path from the ice-free ocean south
654 of Svalbard. Vertical trajectory heights indicate shared transport history and influence by the
655 same emission sources, consistent with Case I.

656 In line with the lower aerosol number concentrations, offline measurements of chemical
657 constituents were also generally lower than in the previous cases. Furthermore, major
658 inorganic ions (**Figure 5c**) were generally similar at the ground and balloon (Cl_{aer}^- : 289 &

659 252 ng m⁻³; SO₄²⁻_{aer}: 66 & 59 ng m⁻³; K⁺_{aer}: 23 & 20 ng m⁻³), with Na⁺_{aer} (53 & 35 ng m⁻³)
660 somewhat higher at the ground. At the Zeppelin Observatory, only Na⁺_{aer} exceeded the
661 detection limit, with a concentration of 38 ng m⁻³, very similar to the value observed at the
662 balloon. This consistency indicates a rather mixed boundary layer. Creamean et al. (2021)
663 analyzed three years of Arctic aerosol vertical distributions using a tethered balloon in Alaska
664 and found that, when a uniform aerosol distribution below clouds was observed, it primarily
665 occurred in autumn, aligning well with Case III.

666 Interestingly, despite the same levels of major inorganic ions, some chemical constituents
667 exhibited increased concentrations at higher altitudes. These included major
668 monosaccharides bound within CCHO (ground & balloon: Glc_{CCHO,aer}: 12.6 & 34 ng m⁻³;
669 Xyl_{CCHO,aer}: 0.57 & 4.4 ng m⁻³; Ara_{CCHO,aer}: below detection limit & 0.97 ng m⁻³), as well as
670 oxalate_{aer} (5.5 & 24 ng m⁻³), Ca²⁺_{aer} (47 & 187 ng m⁻³), and Mg²⁺_{aer} (0.97 & 2.6 ng m⁻³). These
671 elevated concentrations cannot be explained by direct local sea spray emissions or remote
672 source contributions alone, suggesting the involvement of cloud-related enrichment and
673 transformation processes.

674 Soluble Ca²⁺_{aer} and Mg²⁺_{aer} possibly derived from preexisting organic structures in SSA,
675 becoming soluble and detectable after chemical aging. OM-bound Ca²⁺, as already found in
676 Antarctic SSA (Su et al., 2023), may originate from SML-derived polysaccharide gels such as
677 TEPs, and airborne algal cells or fragments, which can release Ca²⁺ and Mg²⁺ through gel
678 dispersion or cell dissolution under the acidic conditions of chemically aged SSA aerosol
679 particles (Aller et al., 2017; Angle et al., 2021; Orellana and Leck, 2015; van Pinxteren et al.,
680 2022; Trainic et al., 2018; Zhu et al., 2014). Since these particles were sampled in cloud water,
681 which contains abundant TEP (van Pinxteren et al., 2022), this mechanism may also explain
682 the elevated CCHO concentrations. Ca²⁺_{aer} can form complexes with oxalate_{aer} (Furukawa and
683 Takahashi, 2011), and oxalic acid increases hygroscopicity, potentially accounting for the high
684 values observed at the balloon in Case III. In addition, secondary in-situ atmospheric or
685 microbial origins, particularly in the aqueous phase, may contribute to CCHO_{aer} and oxalate_{aer}
686 and is discussed in the following section.

687 In summary, Case III demonstrates that certain SSA constituents can vary with altitude due to
688 atmospheric processing following primary emissions and vertical transport.

689 Together, the three cases demonstrate that meteorological conditions can lead to similar,
690 lower, or higher concentrations of the investigated chemical constituents across different
691 altitudes. Porter et al. (2022) observed similar patterns for ice-nucleating particles at the
692 North Pole. They combined their measurements with trajectory analyses and heat sensitivity
693 tests to conclude on aerosol sources. While this effect-based approach gives insights into
694 particle properties, direct chemical analyses, as performed in this study, can further enhance
695 certainty about particle origin and composition relevant for cloud formation.

696 **3.3 Factors affecting SSA constituents beyond local sea-air transfer**

697 *Long-range transport and size-dependent deposition*

698 SSA particles originate from both local and remote marine regions. However, our sampling
699 methods make it challenging to determine the relative contribution of long-range transported
700 SSA constituents, particularly when a local marine source, such as the Kongsfjorden is adjacent
701 to the sampling site and may dominate other marine emissions.

702 As demonstrated in Case II, long-range transport of SSA can become dominant when air
703 masses at elevated altitudes are decoupled from those at the ground. In this case, vertical and
704 horizontal trajectory analysis suggests that the measured SSA constituents may have been
705 emitted and incorporated into the atmosphere approximately 48 hours earlier over the
706 Barents Sea, near Franz Josef Land. Typical removal processes of supermicron particles, such
707 as dry and wet deposition or cloud droplet activation, likely reduced the atmospheric
708 concentrations of major inorganic ions and CCHO_{aer} by one to two orders of magnitude before
709 the arrival of the air masses in Ny-Ålesund (**Figure 5b**).

710 In several balloon-borne TSP filter samples, an elevated $\text{CCHO}_{\text{aer}}/\text{Na}^+_{\text{aer}}$ ratio was observed,
711 most notably on 24 Sep 2021; 03 Oct 2021 (Case III) and 03 Apr 2022 (see **Figure 2d**). These
712 values far exceeded both ground-based aerosol measurements from this study and previously
713 reported values (Zeppenfeld et al., 2021, 2023), particularly for supermicron SSA particles that
714 dominate the TSP mass. A slight increase of this ratio may be explained by a longer
715 atmospheric residence time of these particles. This leads to a relative reduction of
716 supermicron aerosol particles, typically dominated by sea salt (O'Dowd and de Leeuw, 2007),
717 through deposition (Croft et al., 2009; Hoppel et al., 2002). In contrast, submicron aerosol
718 particles, which are rich in surface-active CCHO, remain. This process could lead to a shift of
719 the $\text{CCHO}_{\text{aer}}/\text{Na}^+_{\text{aer}}$ ratios more characteristic of submicron than supermicron particles in the
720 TSP samples of this study, as seen in Case II.

721 However, for the three cases with the most pronounced increases in $\text{CCHO}_{\text{aer}}/\text{Na}^+_{\text{aer}}$ ratios in
722 TSP at higher altitudes (24 Sep 2021; 03 Oct 2021; 03 Apr 2022), absolute CCHO_{aer}
723 concentrations were also elevated (compare **Figures 2b and 2d**). Such increases in absolute
724 concentrations cannot be explained by the selective removal of supermicron particles as
725 hypothesized above. This raises the question of whether the observed CCHO_{aer} concentrations

726 could result from the long-range transport of SSA compounds from a distant marine source
727 with significantly higher CCHO levels than the local Kongsfjorden.

728 Model simulations using FESOM2.1-REcoM3 (Gürses et al., 2023) (**Figure S6**) and field data
729 (Assmy et al., 2023; Feltracco et al., 2021; Grosse et al., 2021; Wietz et al., 2024) confirm that
730 the eastern Fram Strait as well as coastal Svalbard waters are productive and polysaccharide-
731 rich regions. While the FESOM2.1-REcoM3 model does not resolve the SML separately,
732 previous studies have shown significant CCHO enrichment in this layer (Compiano et al., 1993;
733 Engel and Galgani, 2016; Gao et al., 2012; Zäncker et al., 2021), particularly in the productive
734 marginal ice zone (Zeppenfeld et al., 2023). However, in cases of high CCHO_{aer} at higher
735 altitudes in this study, air mass trajectories did not pass over any of these productive marine
736 regions within 48 hours before reaching Svalbard (**Figure S7**). These findings suggest that long-
737 range transport of SSA from more productive remote marine sources is unlikely to explain the
738 elevated CCHO_{aer} concentrations at elevated altitudes within the lower troposphere in Ny-
739 Ålesund, further supporting a predominantly local source or atmospheric in-situ formation.

740 In summary, while long-range transport of SSA constituents at elevated altitudes appears
741 relevant in cases of decoupled atmospheric layers such as in Case II, it may not explain the
742 significantly higher CCHO_{aer} concentrations at high altitudes compared to ground levels.
743 Instead, in-situ formation of CCHO_{aer} could be a more plausible explanation for these
744 observations.

745

746 ***Atmospheric in-situ formation of marine CCHO_{aer}***

747 Bacteria can be transported into and persist in the Arctic atmosphere (Jensen et al., 2022;
748 Šantl-Temkiv et al., 2018), with sources including terrestrial environments and surface
749 seawater, particularly the SML (Aller et al., 2005). Our complementary microbiological
750 sampling during our campaign supported such dynamics by detecting diverse marine bacteria
751 in aerosol particles (Wietz et al., 2025). Some aerosolized taxa, for instance *Polaribacter*,
752 encode multiple genes for CCHO metabolism (Avci et al., 2020) and consistently occur in both
753 Kongsfjorden seawater and atmosphere during the spring bloom (Feltracco et al., 2021). These
754 observations might underpin microbial CCHO transformations in the atmosphere, for instance
755 the production of polysaccharide-based gels as protection against temperature fluctuations,
756 salinity changes, and desiccation (Aller et al., 2005; Ramasamy et al., 2023; Šantl-Temkiv et al.,

757 2022). Under highly humid conditions, especially in the presence of liquid water (such as in
758 Case III), airborne bacteria can become metabolically active (Ervens and Amato, 2020;
759 Haddrell and Thomas, 2017). Atmospheric OM formation, including CCHO, through microbial
760 activity has been documented for cloud water and aerosol particles (Bianco et al., 2019; Klein
761 et al., 2016; Matulová et al., 2014). Although substantial uncertainties remain, Zeppenfeld et
762 al. (2021) estimated, depending on parameter choice, residence times between 20 minutes
763 and several hundred hours during which measurable microbial transformation of
764 carbohydrates in the atmosphere may occur. Consequently, metabolically active bacteria in
765 the atmosphere could explain the increased CCHO_{aer} concentrations observed within or near
766 drizzling clouds in Case III of this study.

767 ***CCHO_{aer} versus oxalate_{aer}: Co-production or atmospheric processing?***

768 Since both combined glucose and combined xylose were consistently detected in CCHO_{aer} of
769 nearly all aerosol samples, we examined their correlation with other atmospheric chemical
770 parameters. We observed a strong correlation between atmospheric xylose in CCHO_{aer} and
771 oxalate_{aer} with an R=0.78 (p<0.001) across all sampling locations and heights (**Figure 7**).
772 Oxalate, the ionic form of oxalic acid, is the most abundant dicarboxylic acid in aerosol
773 particles (Kerminen et al., 1999; Rinaldi et al., 2011), with atmospheric concentrations in this
774 study between <1 and 67 ng m⁻³. The strong correlation raised the question of whether oxalic
775 acid could be chemically linked to combined carbohydrates in aerosol particles.

776 Oxalate_{aer} is known to originate from several primary sources and secondary formation
777 pathways in both terrestrial and anthropogenic environments (Kawamura and Bikkina, 2016;
778 Yang et al., 2022). In remote marine environments, the atmospheric formation of oxalic acid
779 was proposed by Warneck (2003) through the aqueous-phase oxidation of glyoxal and
780 glycolaldehyde, a process also investigated by field measurements inside and above marine
781 clouds (Crahan et al., 2004; Sorooshian et al., 2007) and modeling (Herrmann et al., 2005;
782 Tilgner and Herrmann, 2010). The possible aqueous-phase formation was supported by Case
783 III of this study, where higher oxalate_{aer} concentrations were observed within and in vicinity of
784 clouds compared to ground level. In contrast, in the drier conditions of Cases I and II, oxalate_{aer}
785 levels remained vertically uniform. Additionally, since overall oxalate_{aer} levels at the Old Pier
786 (1.1–10.1 ng m⁻³; mean=4.3±3.5 ng m⁻³) were relatively low compared to the more inland

787 Winch ($<1\text{--}58\text{ ng m}^{-3}$; $\text{mean}=19.8\pm 16.2\text{ ng m}^{-3}$) and elevated altitudes samples ($4.6\text{--}67\text{ ng m}^{-3}$;
788 $\text{mean}=29.6\pm 17.8\text{ ng m}^{-3}$), direct primary oceanic emission was likely not its dominant source.

789

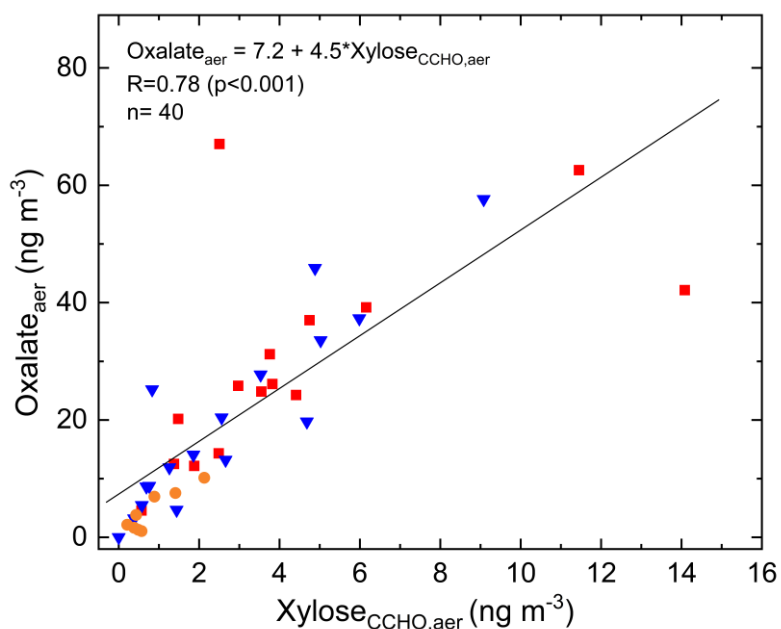


Figure 7. Atmospheric oxalate as a function of xylose in CCHO_{aer} ($R=0.78$; $p<0.001$) measured in TSP from the Old Pier (orange circles), the winch site (blue triangles) and at elevated altitudes (red squares).

798 But what are the precursors of glyoxal and glycolaldehyde, the precursors of oxalic acid? While
799 Warneck (2003) suggested that the anthropogenic volatile organic compounds acetylene and
800 ethene can be transformed to atmospheric glyoxal, other studies suggest the photochemical
801 degradation of marine OM (McNeill, 2015; Sinreich et al., 2010; Turekian et al., 2003; Zhou et
802 al., 2014), with oligo- and polysaccharides representing a known subclass. Although not
803 explicitly measured in this study, previous findings have shown that both CCHO_{aer} (Leck et al.,
804 2013; Zeppenfeld et al., 2021, 2023) and oxalate_{aer} (Guo et al., 2016; Rinaldi et al., 2011;
805 Turekian et al., 2003) are present across both the accumulation and coarse size modes.
806 However, no consistently dominant size mode has been identified, which may support a
807 common mechanism of formation or similar atmospheric processing pathways.

808 Here, based on known chemical reactions, we propose possible atmospheric pathways linking
809 xylose-containing oligo- and polysaccharides as the precursors to oxalate as the final product
810 (**Figure 8**). The initial depolymerization of CCHO presumably occurs either via enzymatic
811 degradation, e.g. by glycoside hydrolases, or acid hydrolysis (Panagiotopoulos and Sempéré,

2005), both of which are plausible in the atmospheric context. Active microbial enzymes have been detected in SSA, often exhibiting activities 1–2 orders of magnitude higher than in bulk seawater (Malfatti et al., 2019). Additionally, SSA particles are known for reaching very low pH levels within minutes after their emissions due to the uptake and reactions with acidic gases, as well as water loss (Angle et al., 2022, 2021). Furthermore, although not explicitly investigated in an atmospheric context, Zhu et al. (2023) observed rapid depolymerization of xylose-containing oligosaccharides into the monosaccharide xylose within minutes in a UV/H₂O₂ system, which generates hydroxyl radicals.

820
821
822
823
824
825
826
827
828
829

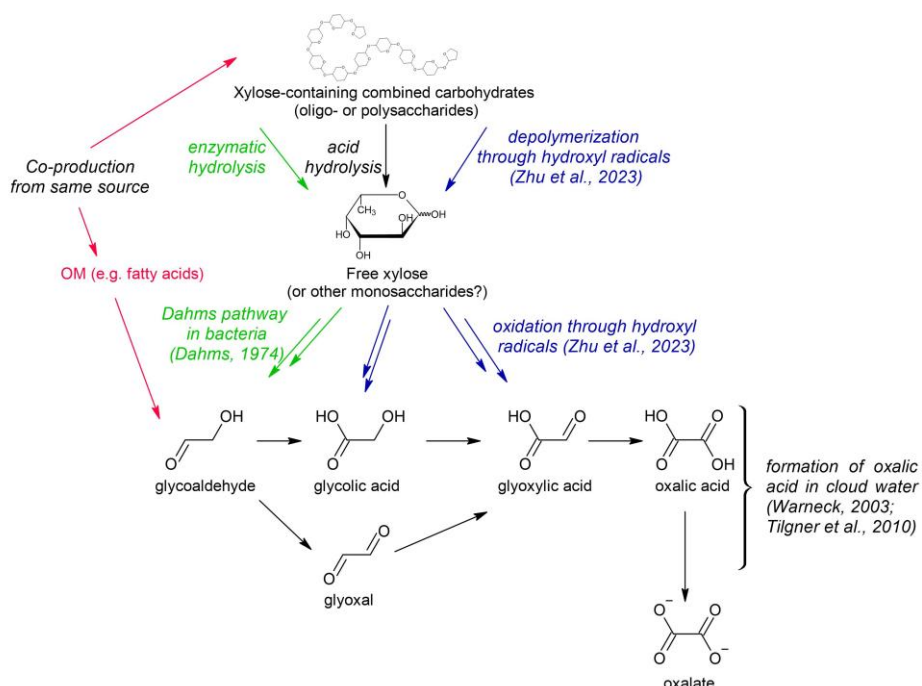


Figure 8. Possible pathways for the formation of atmospheric oxalate from xylose in combined carbohydrates in marine aerosol particles.

With one exception, free xylose was never detected in any aerosol sample of this study. This suggests two possible explanations. First, xylose may have remained bound within the CCHO_{aer} fraction and was not released into its free form. In this case, it would indicate co-emission without a chemical pathway leading to oxalate. Second, free xylose may have been rapidly processed in the atmosphere via reactions described below.

Two potential pathways may link monomeric xylose to precursors of Warneck’s oxalate formation: (1) a follow-up reaction with hydroxyl radicals, where the pyranose ring of xylose is cleaved after the more susceptible glycosidic bonds have been readily broken. Zhu et al.

838 (2023) observed glycolic acid and glyoxylic acid among other products following the UV/H₂O₂
839 treatment of xylooligosaccharides. (2) Bacterial metabolism via the Dahms pathway
840 converting free xylose into pyruvate and glycolaldehyde (Dahms, 1974). However, only few
841 bacteria encode this pathway; and it is highly questionable whether these occur in sufficient
842 atmospheric concentrations for a measurable effect.

843 One indication that direct formation from xylose-containing oligo- and polysaccharides cannot
844 be the sole source of atmospheric oxalate in the marine environment is the discrepancy in
845 concentrations: atmospheric oxalate levels were seven times higher than those of combined
846 xylose. This confirms the involvement of additional precursors or a co-production/co-emission
847 of combined xylose with gaseous precursors, such as isoprene (Carlton et al., 2009; Kawamura
848 and Bikina, 2016), or other primary marine organic matter, such as phytoplankton-derived
849 fatty acids (Kawamura et al., 1996a, b) undergoing photo-oxidation. Further targeted
850 laboratory and modeling studies are needed for clarity.

851 **4. Summary and Atmospheric Implications**

852 In autumn 2021 and spring 2022, we performed balloon-borne measurements of major SSA
853 constituents at Ny-Ålesund (Svalbard). Our evidence demonstrated that both sodium and
854 marine CCHO reach elevated altitudes within the boundary layer, and even the free
855 troposphere as part of aerosol particles. The relationship between ground-level and high-
856 altitude measurements was strongly influenced by meteorological conditions and the mixing
857 state of the lower atmosphere, as discussed in three representative cases. Long-range
858 transport of Na^+_{aer} and CCHO_{aer} from remote marine sources is presumably relevant for high-
859 altitude measurements, especially when the upper air masses were decoupled from the
860 ground. However, in cases of a well-mixed lower atmosphere, the local marine source (here,
861 the Kongsfjorden) was the dominant contributor for atmospheric Na^+_{aer} and CCHO_{aer} . Under
862 very humid conditions particularly in the presence of liquid precipitating clouds, in-situ
863 formation of CCHO_{aer} was observed, possibly linked to microbial metabolism. To establish
864 more generalizable patterns, we recommend further field studies using airborne platforms.

865 The significant correlation between combined xylose within CCHO_{aer} , and $\text{oxalate}_{\text{aer}}$ suggests
866 underlying pathways for oxalic acid formation from combined xylose and other
867 monosaccharide units within CCHO_{aer} ; alternatively, a co-production of xylose-containing
868 oligo- and polysaccharides alongside oxalate precursors.

869 Cloud condensation nuclei and ice-nucleating particles are key drivers in cloud formation,
870 influencing radiative and precipitation properties and, consequently, climate processes.
871 Considerable uncertainties remain regarding the origin and chemical composition of these
872 particles, particularly in remote Arctic regions, which affects the accuracy of climate models.
873 Since marine polysaccharides have been identified as relevant ice-nucleating molecules in the
874 remote marine atmosphere (Hartmann et al., 2025), our findings have implications for cloud
875 microphysics, especially given that these carbohydrates are transported to altitudes relevant
876 for cloud formation. Furthermore, atmospheric processing, as observed here, may alter the
877 ice-nucleating properties of these macromolecules, potentially creating new ice-nucleating
878 particles in-situ or deactivating existing ones.

879 As the Arctic continues to change, expanding ice-free ocean areas will serve as emission
880 sources for SSA particles, influencing cloud properties, and finally the radiative budget.

881 Consequently, our findings contribute to an improved understanding of the complex interplay
882 of environmental processes resulting in Arctic amplification.

883 **Author contributions**

884 SZ wrote the manuscript with input from all co-authors. SZ, JS, CP, HS, BW, MW, and MvP
885 collected field samples in Ny-Ålesund. HS and BW served as principal investigators for balloon
886 operations during the field campaign. SZ conducted the laboratory carbohydrate analyses and
887 data processing. MZ and AB carried out the FESOM2.1-REcoM3 simulations. KE assessed cloud
888 conditions for the case studies using remote sensing data. All co-authors reviewed and
889 commented on the manuscript.

890

891 **Acknowledgments**

892 We would like to express our gratitude to Kings Bay and the AWIPEV staff, with special thanks
893 to the station leader Grégory Tran, for their invaluable support to make this field study
894 possible. We furthermore thank the AWIPEV station's scientific staff in ensuring the
895 availability of high-quality meteorological data. In this context, we like to give special thanks
896 to Fieke Rader and Marion Maturilli. The cloud observations were taken within the project
897 AWIPEV_0016.

898 We also thank the scientific team at the Zeppelin Observatory from NILU and NPI, with special
899 appreciation to Wenche Aas, for their dedicated work in monitoring aerosol data.

900 Furthermore, we acknowledge the entire BELUGA team for their contributions during both
901 the autumn 2021 and spring 2022 campaigns, with special thanks to Thomas Conrath. We also
902 thank Michel Michalkow for preprocessing the CAMP and standard meteorological data
903 collected at BELUGA as part of his Master's thesis. We are grateful to René Rabe for preparing
904 the campaign equipment and to Leon Schmidt for conducting the chemical analysis of
905 inorganic ions.

906 For the FESOM2.1-REcoM3 simulation for this research, the authors gratefully acknowledge
907 the computing time granted by the Resource Allocation Board and provided on the
908 supercomputer Lise and Emmy at NHR@ZIB and NHR@Göttingen as part of the NHR

909 infrastructure. The calculations for this research were conducted with computing resources
910 under the project hbk00084.

911 This research has been supported by the Deutsche Forschungsgemeinschaft (DFG, German
912 Research Foundation, project no. 268020496-TRR 172) within the Transregional Collaborative
913 Research Center “ArctiC Amplification: Climate Relevant Atmospheric and SurfaCe Processes,
914 and Feedback Mechanisms (AC)3” in subprojects A02, B04, C03 and E02. MW was supported
915 by the DFG Priority Program SPP 1158 “Antarctic Research with comparative investigations in
916 Arctic ice areas” (grant 522416631). We thank Johannes Röttenbacher for his constructive
917 feedback on the manuscript.

918

919 **Competing interests**

920 All authors declare no financial or non-financial competing interests. Some authors are
921 members of the editorial board of ACP.

922

923 **Data availability**

924 Chemical data from offline TSP filters are publicly available in PANGAEA for seawater
925 (Zeppenfeld and Schmidt, 2025) and aerosol particles (Zeppenfeld et al., 2025). The
926 microwave radiometer LWP and IWV data are available in PANGAEA (Ebell and Ritter, 2022).
927 The Cloudnet classification and ice water content products (Ebell et al., 2025) can be
928 downloaded via the ACTRIS Cloudnet data portal (<https://cloudnet.fmi.fi>).

929 References

- 930 Aas, W., Berglen, T. F., Eckhardt, S., Fiebig, M., Solberg, S., and Yttri, K. E.: Monitoring of long-range transported air pollutants
931 in Norway. Annual Report 2021., NILU, 2022.
- 932 Aas, W., Eckhardt, S., Solberg, S., and Yttri, K. E.: Monitoring of long-range transported air pollutants in Norway. Annual Report
933 2022., NILU, 2023.
- 934 Akansu, E. F., Dahlke, S., Siebert, H., and Wendisch, M.: Evaluation of methods to determine the surface mixing layer height
935 of the atmospheric boundary layer in the central Arctic during polar night and transition to polar day in cloudless and cloudy
936 conditions, *Atmospheric Chemistry and Physics*, 23, 15473–15489, <https://doi.org/10.5194/acp-23-15473-2023>, 2023.
- 937 Aller, J. Y., Kuznetsova, M. R., Jahns, C. J., and Kemp, P. F.: The sea surface microlayer as a source of viral and bacterial
938 enrichment in marine aerosols, *Journal of Aerosol Science*, 36, 801–812, <https://doi.org/10.1016/j.jaerosci.2004.10.012>,
939 2005.
- 940 Aller, J. Y., Radway, J. C., Kilhau, W. P., Bothe, D. W., Wilson, T. W., Vaillancourt, R. D., Quinn, P. K., Coffman, D. J., Murray,
941 B. J., and Knopf, D. A.: Size-resolved characterization of the polysaccharidic and proteinaceous components of sea spray
942 aerosol, *Atmospheric Environment*, 154, 331–347, <https://doi.org/10.1016/j.atmosenv.2017.01.053>, 2017.
- 943 Alpert, P. A., Kilhau, W. P., O'Brien, R. E., Moffet, R. C., Gilles, M. K., Wang, B., Laskin, A., Aller, J. Y., and Knopf, D. A.: Ice-
944 nucleating agents in sea spray aerosol identified and quantified with a holistic multimodal freezing model, *Science Advances*,
945 8, eabq6842, <https://doi.org/10.1126/sciadv.abq6842>, 2022.
- 946 Aluwihare, L. I., Repeta, D. J., and Chen, R. F.: A major biopolymeric component to dissolved organic carbon in surface sea
947 water, *Nature*, 387, 166–169, <https://doi.org/10.1038/387166a0>, 1997.
- 948 Amore, A., Giardi, F., Becagli, S., Caiazza, L., Mazzola, M., Severi, M., and Traversi, R.: Source apportionment of sulphate in
949 the High Arctic by a 10 yr-long record from Gruevbadet Observatory (Ny-Ålesund, Svalbard Islands), *Atmospheric
950 Environment*, 270, 118890, <https://doi.org/10.1016/j.atmosenv.2021.118890>, 2022.
- 951 Angle, K., Grassian, V. H., and Ault, A. P.: The rapid acidification of sea spray aerosols, *Physics today*, 75, 58–59,
952 <https://doi.org/10.1063/PT.3.4926>, 2022.
- 953 Angle, K. J., Crocker, D. R., Simpson, R. M. C., Mayer, K. J., Garofalo, L. A., Moore, A. N., Garcia, S. L. M., Or, V. W., Srinivasan,
954 S., Farhan, M., Sauer, J. S., Lee, C., Pothier, M. A., Farmer, D. K., Martz, T. R., Bertram, T. H., Cappa, C. D., Prather, K. A., and
955 Grassian, V. H.: Acidity across the interface from the ocean surface to sea spray aerosol, *PNAS*, 118, 1–6,
956 <https://doi.org/10.1073/pnas.2018397118>, 2021.
- 957 Arnosti, C., Wietz, M., Brinkhoff, T., Hehemann, J.-H., Probandt, D., Zeugner, L., and Amann, R.: The Biogeochemistry of
958 Marine Polysaccharides: Sources, Inventories, and Bacterial Drivers of the Carbohydrate Cycle, *Ann Rev Mar Sci*, 13, 81–108,
959 <https://doi.org/10.1146/annurev-marine-032020-012810>, 2021.
- 960 Assmy, P., Cecilie Kvernvik, A., Hop, H., Hoppe, C. J. M., Chierici, M., David T., D., Duarte, P., Fransson, A., García, L. M., Patuła,
961 W., Kwaśniewski, S., Maturilli, M., Pavlova, O., Tatarek, A., Wiktor, J. M., Wold, A., Wolf, K. K. E., and Bailey, A.: Seasonal
962 plankton dynamics in Kongsfjorden during two years of contrasting environmental conditions, *Progress in Oceanography*,
963 213, 102996, <https://doi.org/10.1016/j.pocean.2023.102996>, 2023.
- 964 Avci, B., Krüger, K., Fuchs, B. M., Teeling, H., and Amann, R. I.: Polysaccharide niche partitioning of distinct *Polaribacter* clades
965 during North Sea spring algal blooms, *ISME J*, 14, 1369–1383, <https://doi.org/10.1038/s41396-020-0601-y>, 2020.
- 966 Barthelmeß, T., Cristi, A., Deppeler, S., Safi, K., Sellegrì, K., Law, C. S., and Engel, A.: Pronounced Diel Cycling of Dissolved
967 Carbohydrates and Amino Acids in the Surface Ocean and across Diverse Regimes, *Environ. Sci. Technol.*, 59, 419–429,
968 <https://doi.org/10.1021/acs.est.4c00491>, 2025.
- 969 Becker, S., Tebben, J., Coffinet, S., Wiltshire, K., Iversen, M. H., Harder, T., Hinrichs, K.-U., and Hehemann, J.-H.: Laminarin is
970 a major molecule in the marine carbon cycle, *PNAS*, 117, 6599–6607, <https://doi.org/10.1073/pnas.1917001117>, 2020.
- 971 Bianco, A., Deguillaume, L., Chaumerliac, N., Vařtilingom, M., Wang, M., Delort, A.-M., and Bridoux, M. C.: Effect of
972 endogenous microbiota on the molecular composition of cloud water: a study by Fourier-transform ion cyclotron resonance
973 mass spectrometry (FT-ICR MS), *Sci Rep*, 9, 1–12, <https://doi.org/10.1038/s41598-019-44149-8>, 2019.
- 974 Bischof, K., Convey, P., Duarte, P., Gattuso, J.-P., Granberg, M., Hop, H., Hoppe, C., Jiménez, C., Lisitsyn, L., Martínez, B.,
975 Roleda, M. Y., Thor, P., Wiktor, J. M., and Gabrielsen, G. W.: Kongsfjorden as Harbinger of the Future Arctic: Knowns,
976 Unknowns and Research Priorities, in: *The Ecosystem of Kongsfjorden, Svalbard*, edited by: Hop, H. and Wiencke, C., Springer
977 International Publishing, Cham, 537–562, https://doi.org/10.1007/978-3-319-46425-1_14, 2019.
- 978 Bivand, R., Pebesma, E., and Gomez-Rubio, V.: *Applied spatial data analysis with R*, Springer, 2013.
- 979 Bivand, R., Keitt, T., and Rowlingson, B.: *rgdal: Bindings for the “Geospatial” Data Abstraction Library*, R package version 1.5-
980 32, 2022.

981 Borch, N. H. and Kirchman, D. L.: Concentration and composition of dissolved combined neutral sugars (polysaccharides) in
982 seawater determined by HPLC-PAD, *Marine Chemistry*, 57, 85–95, [https://doi.org/10.1016/S0304-4203\(97\)00002-9](https://doi.org/10.1016/S0304-4203(97)00002-9), 1997.

983 Brownrigg, M. R.: Package ‘mapdata, R package version 2.3.1, 2013.

984 Brownrigg, M. R.: maps: Draw Geographical Maps, R package version 3.4.2, 2023.

985 Browse, J., Carslaw, K. S., Mann, G. W., Birch, C. E., Arnold, S. R., and Leck, C.: The complex response of Arctic aerosol to sea-
986 ice retreat, *Atmospheric Chemistry and Physics*, 14, 7543–7557, <https://doi.org/10.5194/acp-14-7543-2014>, 2014.

987 Burns, W. G., Marchetti, A., and Ziervogel, K.: Enhanced formation of transparent exopolymer particles (TEP) under
988 turbulence during phytoplankton growth, *J Plankton Res*, 41, 349–361, <https://doi.org/10.1093/plankt/fbz018>, 2019.

989 Burrows, S. M., Ogunro, O., Frossard, A., Russell, L. M., Rasch, P. J., and Elliott, S.: A Physically Based Framework for Modelling
990 the Organic Fractionation of Sea Spray Aerosol from Bubble Film Langmuir Equilibria, *Atmospheric Chemistry and Physics*,
991 14(24):13601–13629, <https://doi.org/10.5194/acp-14-13601-2014>, 2014.

992 Cai, Q., Wang, J., Beletsky, D., Overland, J., Ikeda, M., and Wan, L.: Accelerated decline of summer Arctic sea ice during 1850–
993 2017 and the amplified Arctic warming during the recent decades, *Environ. Res. Lett.*, 16, 034015,
994 <https://doi.org/10.1088/1748-9326/abdb5f>, 2021.

995 Carlton, A. G., Wiedinmyer, C., and Kroll, J. H.: A review of Secondary Organic Aerosol (SOA) formation from isoprene,
996 *Atmospheric Chemistry and Physics*, 9, 4987–5005, <https://doi.org/10.5194/acp-9-4987-2009>, 2009.

997 Carslaw, D. C. and Ropkins, K.: openair --- An R package for air quality data analysis, *Environmental Modelling & Software*,
998 27–28, 52–61, 2012.

999 Chang, L., Song, S., Feng, G., Zhang, Y., and Gao, G.: Assessment of the Uncertainties in Arctic Low-Level Temperature
1000 Inversion Characteristics in Radio Occultation Observations, *IEEE Transactions on Geoscience and Remote Sensing*, 55, 1793–
1001 1803, <https://doi.org/10.1109/TGRS.2016.2633461>, 2017.

1002 Chi, J. W., Li, W. J., Zhang, D. Z., Zhang, J. C., Lin, Y. T., Shen, X. J., Sun, J. Y., Chen, J. M., Zhang, X. Y., Zhang, Y. M., and Wang,
1003 W. X.: Sea salt aerosols as a reactive surface for inorganic and organic acidic gases in the Arctic troposphere, *Atmospheric
1004 Chemistry and Physics*, 15, 11341–11353, <https://doi.org/10.5194/acp-15-11341-2015>, 2015.

1005 Compiano, A.-M., Romano, J.-C., Garabetian, F., Laborde, P., and de la Giraudière, I.: Monosaccharide composition of
1006 particulate hydrolysable sugar fraction in surface microlayers from brackish and marine waters, *Marine Chemistry*, 42, 237–
1007 251, [https://doi.org/10.1016/0304-4203\(93\)90015-G](https://doi.org/10.1016/0304-4203(93)90015-G), 1993.

1008 Crahan, K. K., Hegg, D., Covert, D. S., and Jonsson, H.: An exploration of aqueous oxalic acid production in the coastal marine
1009 atmosphere, *Atmospheric Environment*, 38, 3757–3764, <https://doi.org/10.1016/j.atmosenv.2004.04.009>, 2004.

1010 Creamean, J. M., de Boer, G., Telg, H., Mei, F., Dexheimer, D., Shupe, M. D., Solomon, A., and McComiskey, A.: Assessing the
1011 vertical structure of Arctic aerosols using balloon-borne measurements, *Atmospheric Chemistry and Physics*, 21, 1737–1757,
1012 <https://doi.org/10.5194/acp-21-1737-2021>, 2021.

1013 Croft, B., Lohmann, U., Martin, R. V., Stier, P., Wurzler, S., Feichter, J., Posselt, R., and Ferrachat, S.: Aerosol size-dependent
1014 below-cloud scavenging by rain and snow in the ECHAM5-HAM, *Atmospheric Chemistry and Physics*, 9, 4653–4675,
1015 <https://doi.org/10.5194/acp-9-4653-2009>, 2009.

1016 Cunliffe, M. and Wurl, O.: Guide to best practices to study the ocean’s surface., *Marine Biological Association of the United
1017 Kingdom for SCOR*, 2014.

1018 Dahms, A. S.: 3-Deoxy-D-pentulosonic acid aldolase and its role in a new pathway of D-xylose degradation, *Biochemical and
1019 Biophysical Research Communications*, 60, 1433–1439, [https://doi.org/10.1016/0006-291X\(74\)90358-1](https://doi.org/10.1016/0006-291X(74)90358-1), 1974.

1020 Dekhtyareva, A., Holmén, K., Maturilli, M., Hermansen, O., and Graversen, R.: Effect of seasonal mesoscale and microscale
1021 meteorological conditions in Ny-Ålesund on results of monitoring of long-range transported pollution, *Polar Research*, 2018.

1022 DeMott, P. J., Hill, T. C. J., McCluskey, C. S., Prather, K. A., Collins, D. B., Sullivan, R. C., Ruppel, M. J., Mason, R. H., Irish, V. E.,
1023 Lee, T., Hwang, C. Y., Rhee, T. S., Snider, J. R., McMeeking, G. R., Dhaniyala, S., Lewis, E. R., Wentzell, J. J. B., Abbatt, J., Lee,
1024 C., Sultana, C. M., Ault, A. P., Axson, J. L., Martinez, M. D., Venero, I., Santos-Figueroa, G., Stokes, M. D., Deane, G. B., Mayol-
1025 Bracero, O. L., Grassian, V. H., Bertram, T. H., Bertram, A. K., Moffett, B. F., and Franc, G. D.: Sea spray aerosol as a unique
1026 source of ice nucleating particles, *PNAS*, 113, 5797–5803, <https://doi.org/10.1073/pnas.1514034112>, 2016.

1027 Dusek, U., Frank, G. P., Hildebrandt, L., Curtius, J., Schneider, J., Walter, S., Chand, D., Drewnick, F., Hings, S., Jung, D.,
1028 Borrmann, S., and Andreae, M. O.: Size Matters More Than Chemistry for Cloud-Nucleating Ability of Aerosol Particles,
1029 *Science*, 312, 1375–1378, <https://doi.org/10.1126/science.1125261>, 2006.

1030 Ebell, K. and Ritter, C.: HATPRO microwave radiometer measurements at AWIPEV, Ny-Ålesund (2019-2021), PANGAEA,
1031 <https://doi.org/10.1594/PANGAEA.943004>, 2022.

1032 Ebell, K., Maturilli, M., Ritter, C., and O’Connor, E.: Custom collection of classification, and ice water content data from Ny-
1033 Ålesund between 27 Sep and 12 Nov 2021, ACTRIS Cloud remote sensing data centre unit (CLU),
1034 <https://doi.org/10.60656/5598100185854c01>, 2025.

- 1035 Egerer, U., Ehrlich, A., Gottschalk, M., Griesche, H., Neggers, R. A. J., Siebert, H., and Wendisch, M.: Case study of a humidity
1036 layer above Arctic stratocumulus and potential turbulent coupling with the cloud top, *Atmospheric Chemistry and Physics*,
1037 21, 6347–6364, <https://doi.org/10.5194/acp-21-6347-2021>, 2021.
- 1038 Egerer, U., Siebert, H., Hellmuth, O., and Sørensen, L. L.: The role of a low-level jet for stirring the stable atmospheric surface
1039 layer in the Arctic, *Atmospheric Chemistry and Physics*, 23, 15365–15373, <https://doi.org/10.5194/acp-23-15365-2023>, 2023.
- 1040 Engel, A.: Distribution of transparent exopolymer particles (TEP) in the northeast Atlantic Ocean and their potential
1041 significance for aggregation processes, *Deep Sea Research Part I: Oceanographic Research Papers*, 51, 83–92,
1042 <https://doi.org/10.1016/j.dsr.2003.09.001>, 2004.
- 1043 Engel, A. and Galgani, L.: The organic sea-surface microlayer in the upwelling region off the coast of Peru and potential
1044 implications for air–sea exchange processes, *Biogeosciences (BG)*, 13, 989–1007, <https://doi.org/10.5194/bg-13-989-2016>,
1045 2016.
- 1046 Engel, A. and Händel, N.: A novel protocol for determining the concentration and composition of sugars in particulate and in
1047 high molecular weight dissolved organic matter (HMW-DOM) in seawater, *Marine Chemistry*, 127, 180–191,
1048 <https://doi.org/10.1016/j.marchem.2011.09.004>, 2011.
- 1049 Engel, A., Thoms, S., Riebesell, U., Rochelle-Newall, E., and Zondervan, I.: Polysaccharide aggregation as a potential sink of
1050 marine dissolved organic carbon, *Nature*, 428, 929–932, <https://doi.org/10.1038/nature02453>, 2004.
- 1051 Engel, A., Harlay, J., Piontek, J., and Chou, L.: Contribution of combined carbohydrates to dissolved and particulate organic
1052 carbon after the spring bloom in the northern Bay of Biscay (North-Eastern Atlantic Ocean), *Continental Shelf Research*, 45,
1053 42–53, <https://doi.org/10.1016/j.csr.2012.05.016>, 2012.
- 1054 Ervens, B. and Amato, P.: The global impact of bacterial processes on carbon mass, *Atmospheric Chemistry & Physics*, 20,
1055 1777–1794, <https://doi.org/10.5194/acp-20-1777-2020>, 2020.
- 1056 Esau, I. and Repina, I.: Wind Climate in Kongsfjorden, Svalbard, and Attribution of Leading Wind Driving Mechanisms through
1057 Turbulence-Resolving Simulations, *Advances in Meteorology*, 2012, 568454, <https://doi.org/10.1155/2012/568454>, 2012.
- 1058 Fabiano, M., Povero, P., and Danovaro, R.: Distribution and composition of particulate organic matter in the Ross Sea
1059 (Antarctica), *Polar Biol*, 13, 525–533, <https://doi.org/10.1007/BF00236394>, 1993.
- 1060 Facchini, M. C., Rinaldi, M., Decesari, S., Carbone, C., Finessi, E., Mircea, M., Fuzzi, S., Ceburnis, D., Flanagan, R., Nilsson, E. D.,
1061 Leeuw, G. de, Martino, M., Woeltjen, J., and O’Dowd, C. D.: Primary submicron marine aerosol dominated by insoluble organic
1062 colloids and aggregates, *Geophysical Research Letters*, 35, 1–5, <https://doi.org/10.1029/2008GL034210>, 2008.
- 1063 Farmer, D. K., Cappa, C. D., and Kreidenweis, S. M.: Atmospheric Processes and Their Controlling Influence on Cloud
1064 Condensation Nuclei Activity, *Chem. Rev.*, 115, 4199–4217, <https://doi.org/10.1021/cr5006292>, 2015.
- 1065 Farmer, D. K., Boedicker, E. K., and DeBolt, H. M.: Dry Deposition of Atmospheric Aerosols: Approaches, Observations, and
1066 Mechanisms, *Annual Review of Physical Chemistry*, 72, 375–397, <https://doi.org/10.1146/annurev-physchem-090519-034936>, 2021.
- 1068 Feltracco, M., Barbaro, E., Hoppe, C. J. M., Wolf, K. K. E., Spolaor, A., Layton, R., Keuschnig, C., Barbante, C., Gambaro, A., and
1069 Larose, C.: Airborne bacteria and particulate chemistry capture Phytoplankton bloom dynamics in an Arctic fjord, *Atmospheric
1070 Environment*, 256, 118458, <https://doi.org/10.1016/j.atmosenv.2021.118458>, 2021.
- 1071 Fomba, K. W., Müller, K., van Pinxteren, D., Poulain, L., van Pinxteren, M., and Herrmann, H.: Long-term chemical
1072 characterization of tropical and marine aerosols at the Cape Verde Atmospheric Observatory (CVAO) from 2007 to 2011,
1073 *Atmospheric Chemistry and Physics*, 14, 8883–8904, <https://doi.org/10.5194/acp-14-8883-2014>, 2014.
- 1074 Francis, J. A. and Wu, B.: Why has no new record-minimum Arctic sea-ice extent occurred since September 2012?, *Environ.
1075 Res. Lett.*, 15, 114034, <https://doi.org/10.1088/1748-9326/abc047>, 2020.
- 1076 Freud, E., Krejci, R., Tunved, P., Leaitch, R., Nguyen, Q. T., Massling, A., Skov, H., and Barrie, L.: Pan-Arctic aerosol number size
1077 distributions: seasonality and transport patterns, *Atmospheric Chemistry and Physics*, 17, 8101–8128,
1078 <https://doi.org/10.5194/acp-17-8101-2017>, 2017.
- 1079 Furukawa, T. and Takahashi, Y.: Oxalate metal complexes in aerosol particles: implications for the hygroscopicity of oxalate-
1080 containing particles, *Atmos. Chem. Phys.*, 11, 4289–4301, <https://doi.org/10.5194/acp-11-4289-2011>, 2011.
- 1081 Gantt, B., Meskhidze, N., Facchini, M. C., Rinaldi, M., Ceburnis, D., and O’Dowd, C. D.: Wind speed dependent size-resolved
1082 parameterization for the organic mass fraction of sea spray aerosol, *Atmospheric Chemistry and Physics*, 11, 8777–8790,
1083 <https://doi.org/10.5194/acp-11-8777-2011>, 2011.
- 1084 Gao, Q., Leck, C., Rauschenberg, C., and Matrai, P. A.: On the chemical dynamics of extracellular polysaccharides in the high
1085 Arctic surface microlayer, *Ocean Science*, 8, 401–418, <https://doi.org/10.5194/os-8-401-2012>, 2012.
- 1086 Gierens, R., Kneifel, S., Shupe, M. D., Ebell, K., Maturilli, M., and Löhnert, U.: Low-level mixed-phase clouds in a complex Arctic
1087 environment, *Atmospheric Chemistry and Physics*, 20, 3459–3481, <https://doi.org/10.5194/acp-20-3459-2020>, 2020.

1088 Goldberg, S. J., Carlson, C. A., Brzezinski, M., Nelson, N. B., and Siegel, D. A.: Systematic removal of neutral sugars within
1089 dissolved organic matter across ocean basins, *Geophysical Research Letters*, 38, 1–7,
1090 <https://doi.org/10.1029/2011GL048620>, 2011.

1091 Grawe, S., Jentzsch, C., Schaefer, J., Wex, H., Mertes, S., and Stratmann, F.: Next-generation ice-nucleating particle sampling
1092 on board aircraft: characterization of the High-volume flow aERosol particle filter sAmplifier (HERA), *Atmospheric Measurement
1093 Techniques*, 16, 4551–4570, <https://doi.org/10.5194/amt-16-4551-2023>, 2023.

1094 Grolemond, G. and Wickham, H.: Dates and Times Made Easy with lubridate, *Journal of Statistical Software*, 40, 1–25, 2011.

1095 Grosse, J., Nöthig, E.-M., Torres-Valdés, S., and Engel, A.: Summertime Amino Acid and Carbohydrate Patterns in Particulate
1096 and Dissolved Organic Carbon Across Fram Strait, *Front. Mar. Sci.*, 8, <https://doi.org/10.3389/fmars.2021.684675>, 2021.

1097 Guo, T., Li, K., Zhu, Y., Gao, H., and Yao, X.: Concentration and size distribution of particulate oxalate in marine and coastal
1098 atmospheres – Implication for the increased importance of oxalate in nanometer atmospheric particles, *Atmospheric
1099 Environment*, 142, 19–31, <https://doi.org/10.1016/j.atmosenv.2016.07.026>, 2016.

1100 Gürses, Ö., Oziel, L., Karakuş, O., Sidorenko, D., Völker, C., Ye, Y., Zeising, M., Butzin, M., and Hauck, J.: Ocean biogeochemistry
1101 in the coupled ocean–sea ice–biogeochemistry model FESOM2.1–REcoM3, *Geoscientific Model Development*, 16, 4883–
1102 4936, <https://doi.org/10.5194/gmd-16-4883-2023>, 2023.

1103 Haddrell, A. E. and Thomas, R. J.: Aerobiology: Experimental Considerations, Observations, and Future Tools, *Appl. Environ.
1104 Microbiol.*, 83, 1–15, <https://doi.org/10.1128/AEM.00809-17>, 2017.

1105 Hansell, D. A.: Recalcitrant Dissolved Organic Carbon Fractions, *Annual Review of Marine Science*, 5, 421–445,
1106 <https://doi.org/10.1146/annurev-marine-120710-100757>, 2013.

1107 Hara, K., Yamagata, S., Yamanouchi, T., Sato, K., Herber, A., Iwasaka, Y., Nagatani, M., and Nakata, H.: Mixing states of
1108 individual aerosol particles in spring Arctic troposphere during ASTAR 2000 campaign, *Journal of Geophysical Research:
1109 Atmospheres*, 108, 1–12, <https://doi.org/10.1029/2002JD002513>, 2003.

1110 Hartmann, S., Schrödner, R., Hassett, B. T., Hartmann, M., van Pinxteren, M., Fomba, K. W., Stratmann, F., Herrmann, H.,
1111 Pöhlker, M., and Zeppenfeld, S.: Polysaccharides—Important Constituents of Ice-Nucleating Particles of Marine Origin,
1112 *Environ. Sci. Technol.*, 59, 5098–5108, <https://doi.org/10.1021/acs.est.4c08014>, 2025.

1113 Hasenecz, E., Jayarathne, T., Pendergraft, M. A., Santander, M. V., Mayer, K. J., Sauer, J., Lee, C., Gibson, W. S., Kruse, S. M.,
1114 Malfatti, F., Prather, K. A., and Stone, E. A.: Marine bacteria affect saccharide enrichment in sea spray aerosol during a
1115 phytoplankton bloom, *ACS Earth Space Chem.*, 4, 1638–1649, <https://doi.org/10.1021/acsearthspacechem.0c00167>, 2020.

1116 Hasenecz, E. S., Kaluarachchi, C. P., Lee, H. D., Tivanski, A. V., and Stone, E. A.: Saccharide Transfer to Sea Spray Aerosol
1117 Enhanced by Surface Activity, Calcium, and Protein Interactions, *ACS Earth Space Chem.*, 3, 2539–2548,
1118 <https://doi.org/10.1021/acsearthspacechem.9b00197>, 2019.

1119 Herrmann, H., Tilgner, A., Barzagli, P., Majdik, Z., Gligorovski, S., Poulain, L., and Monod, A.: Towards a more detailed
1120 description of tropospheric aqueous phase organic chemistry: CAPRAM 3.0, *Atmospheric Environment*, 39, 4351–4363,
1121 <https://doi.org/10.1016/j.atmosenv.2005.02.016>, 2005.

1122 Heutte, B., Bergner, N., Angot, H., Pernov, J. B., Dada, L., Mirrielees, J. A., Beck, I., Baccarini, A., Boyer, M., Creamean, J. M.,
1123 Daellenbach, K. R., El Haddad, I., Frey, M. M., Henning, S., Laurila, T., Moschos, V., Petäjä, T., Pratt, K. A., Quéléver, L. L. J.,
1124 Shupe, M. D., Zieger, P., Jokinen, T., and Schmale, J.: Observations of high-time-resolution and size-resolved aerosol chemical
1125 composition and microphysics in the central Arctic: implications for climate-relevant particle properties, *Atmospheric
1126 Chemistry and Physics*, 25, 2207–2241, <https://doi.org/10.5194/acp-25-2207-2025>, 2025.

1127 Hijmans, R. J.: raster: Geographic Data Analysis and Modeling, R package version 3.6-26, 2023.

1128 Hill, T. C. J., Malfatti, F., McCluskey, C. S., Schill, G. P., Santander, M. V., Moore, K. A., Rauker, A. M., Perkins, R. J., Celussi, M.,
1129 Levin, E. J. T., Suski, K. J., Cornwell, G. C., Lee, C., Negro, P. D., Kreidenweis, S. M., Prather, K. A., and DeMott, P. J.: Resolving
1130 the controls over the production and emission of ice-nucleating particles in sea spray, *Environ. Sci.: Atmos.*,
1131 <https://doi.org/10.1039/D2EA00154C>, 2023.

1132 Hoffman, E. J. and Duce, R. A.: Factors influencing the organic carbon content of marine aerosols: A laboratory study, *Journal
1133 of Geophysical Research (1896-1977)*, 81, 3667–3670, <https://doi.org/10.1029/JC081i021p03667>, 1976.

1134 Hogan, R. J., Mittermaier, M. P., and Illingworth, A. J.: The Retrieval of Ice Water Content from Radar Reflectivity Factor and
1135 Temperature and Its Use in Evaluating a Mesoscale Model, *Journal of Applied Meteorology and Climatology*, 45, 301–317,
1136 <https://doi.org/10.1175/JAM2340.1>, 2006.

1137 Hoppel, W. A., Frick, G. M., and Fitzgerald, J. W.: Surface source function for sea-salt aerosol and aerosol dry deposition to
1138 the ocean surface, *Journal of Geophysical Research: Atmospheres*, 107, AAC 7-1-AAC 7-17,
1139 <https://doi.org/10.1029/2001JD002014>, 2002.

1140 Illingworth, A. J., Hogan, R. J., O’Connor, E. J., Bouniol, D., Brooks, M. E., Delanoé, J., Donovan, D. P., Eastment, J. D., Gaussiat,
1141 N., Goddard, J. W. F., Haefelin, M., Baltink, H. K., Krasnov, O. A., Pelon, J., Piriou, J.-M., Protat, A., Russchenberg, H. W. J.,
1142 Seifert, A., Tompkins, A. M., Zadelhoff, G.-J. van, Vinit, F., Willén, U., Wilson, D. R., and Wrench, C. L.: Cloudnet: Continuous

- 1143 Evaluation of Cloud Profiles in Seven Operational Models Using Ground-Based Observations, *Bulletin of the American*
1144 *Meteorological Society*, 88, 883–898, <https://doi.org/10.1175/BAMS-88-6-883>, 2007.
- 1145 Ittekkot, V., Brockmann, U., Michaelis, W., and Degens, E. T.: Dissolved free and combined carbohydrates during a
1146 phytoplankton bloom in the northern North Sea, *Marine Ecology Progress Series*, 4, 299–305, 1981.
- 1147 Jayarathne, T., Sultana, C. M., Lee, C., Malfatti, F., Cox, J. L., Pendergraft, M. A., Moore, K. A., Azam, F., Tivanski, A. V., Cappa,
1148 C. D., Bertram, T. H., Grassian, V. H., Prather, K. A., and Stone, E. A.: Enrichment of Saccharides and Divalent Cations in Sea
1149 Spray Aerosol During Two Phytoplankton Blooms, *Environ Sci Technol*, 50, 11511–11520,
1150 <https://doi.org/10.1021/acs.est.6b02988>, 2016.
- 1151 Jensen, L. Z., Glasius, M., Gryning, S.-E., Massling, A., Finster, K., and Šantl-Temkiv, T.: Seasonal Variation of the Atmospheric
1152 Bacterial Community in the Greenlandic High Arctic Is Influenced by Weather Events and Local and Distant Sources, *Front.*
1153 *Microbiol.*, 13, <https://doi.org/10.3389/fmicb.2022.909980>, 2022.
- 1154 Kang, H., Jung, C. H., Lee, B. Y., Krejci, R., Heslin-Rees, D., Aas, W., and Yoon, Y. J.: Aerosol hygroscopicity influenced by
1155 seasonal chemical composition variations in the Arctic region, *Journal of Aerosol Science*, 106551,
1156 <https://doi.org/10.1016/j.jaerosci.2025.106551>, 2025.
- 1157 Kanji, Z. A., Ladino, L. A., Wex, H., Boose, Y., Burkert-Kohn, M., Cziczo, D. J., and Krämer, M.: Overview of Ice Nucleating
1158 Particles, *Meteorological Monographs*, 58, 1.1-1.33, <https://doi.org/10.1175/AMSMONOGRAPHS-D-16-0006.1>, 2017.
- 1159 Karl, M., Leck, C., Rad, F. M., Bäcklund, A., Lopez-Aparicio, S., and Heintzenberg, J.: New insights in sources of the sub-
1160 micrometre aerosol at Mt. Zeppelin observatory (Spitsbergen) in the year 2015, *Tellus B: Chemical and Physical Meteorology*,
1161 71, 1613143, <https://doi.org/10.1080/16000889.2019.1613143>, 2019.
- 1162 Kawamura, K. and Bikkina, S.: A review of dicarboxylic acids and related compounds in atmospheric aerosols: Molecular
1163 distributions, sources and transformation, *Atmospheric Research*, 170, 140–160,
1164 <https://doi.org/10.1016/j.atmosres.2015.11.018>, 2016.
- 1165 Kawamura, K., Kasukabe, H., and Barrie, L. A.: Source and reaction pathways of dicarboxylic acids, ketoacids and dicarbonyls
1166 in arctic aerosols: One year of observations, *Atmospheric Environment*, 30, 1709–1722, [https://doi.org/10.1016/1352-2310\(95\)00395-9](https://doi.org/10.1016/1352-2310(95)00395-9), 1996a.
- 1168 Kawamura, K., Sempéré, R., Imai, Y., Fujii, Y., and Hayashi, M.: Water soluble dicarboxylic acids and related compounds in
1169 Antarctic aerosols, *Journal of Geophysical Research: Atmospheres*, 101, 18721–18728, <https://doi.org/10.1029/96JD01541>,
1170 1996b.
- 1171 Keene, W. C., Pszenny, A. A. P., Galloway, J. N., and Hawley, M. E.: Sea-salt corrections and interpretation of constituent ratios
1172 in marine precipitation, *Journal of Geophysical Research*, 91, 6647–6658, <https://doi.org/10.1029/JD091iD06p06647>, 1986.
- 1173 Keene, W. C., Long, M. S., Reid, J. S., Frossard, A. A., Kieber, D. J., Maben, J. R., Russell, L. M., Kinsey, J. D., Quinn, P. K., and
1174 Bates, T. S.: Factors That Modulate Properties of Primary Marine Aerosol Generated From Ambient Seawater on Ships at Sea,
1175 *Journal of Geophysical Research: Atmospheres*, 122, 11,961-11,990, <https://doi.org/10.1002/2017JD026872>, 2017.
- 1176 Kerminen, V.-M., Teinilä, K., Hillamo, R., and Mäkelä, T.: Size-segregated chemistry of particulate dicarboxylic acids in the
1177 Arctic atmosphere, *Atmospheric Environment*, 33, 2089–2100, [https://doi.org/10.1016/S1352-2310\(98\)00350-1](https://doi.org/10.1016/S1352-2310(98)00350-1), 1999.
- 1178 Khadem, H. E.: *Carbohydrate Chemistry: Monosaccharides and Their Oligomers*, Elsevier, 267 pp., 2012.
- 1179 Kharbush, J. J., Close, H. G., Van Mooy, B. A. S., Arnosti, C., Smittenberg, R. H., Le Moigne, F. A. C., Mollenhauer, G., Scholz-
1180 Böttcher, B., Obrecht, I., Koch, B. P., Becker, K., Iversen, M. H., and Mohr, W.: Particulate Organic Carbon Deconstructed:
1181 Molecular and Chemical Composition of Particulate Organic Carbon in the Ocean, *Frontiers in Marine Science*, 7, Art.Nr. 518,
1182 <https://doi.org/10.3389/fmars.2020.00518>, 2020.
- 1183 Kirchman, D. L., Meon, B., Ducklow, H. W., Carlson, C. A., Hansell, D. A., and Steward, G. F.: Glucose fluxes and concentrations
1184 of dissolved combined neutral sugars (polysaccharides) in the Ross Sea and Polar Front Zone, Antarctica, *Deep Sea Research*
1185 *Part II: Topical Studies in Oceanography*, 48, 4179–4197, [https://doi.org/10.1016/S0967-0645\(01\)00085-6](https://doi.org/10.1016/S0967-0645(01)00085-6), 2001.
- 1186 Klein, A. M., Bohannon, B. J. M., Jaffe, D. A., Levin, D. A., and Green, J. L.: Molecular Evidence for Metabolically Active Bacteria
1187 in the Atmosphere, *Front. Microbiol.*, 7, 772, <https://doi.org/10.3389/fmicb.2016.00772>, 2016.
- 1188 Köllner, F., Schneider, J., Willis, M. D., Klimach, T., Helleis, F., Bozem, H., Kunkel, D., Hoor, P., Burkart, J., Leaitch, W. R.,
1189 Aliabadi, A. A., Abbatt, J. P. D., Herber, A. B., and Borrmann, S.: Particulate trimethylamine in the summertime Canadian high
1190 Arctic lower troposphere, *Atmospheric Chemistry and Physics*, 17, 13747–13766, <https://doi.org/10.5194/acp-17-13747-2017>, 2017.
- 1192 Leck, C., Gao, Q., Mashayekhy Rad, F., and Nilsson, U.: Size-resolved atmospheric particulate polysaccharides in the high
1193 summer Arctic, *Atmospheric Chemistry and Physics*, 13, 12573–12588, <https://doi.org/10.5194/acp-13-12573-2013>, 2013.
- 1194 Leon-Marcos, A., Zeising, M., van Pinxteren, M., Zeppenfeld, S., Bracher, A., Barbaro, E., Engel, A., Feltracco, M., Tegen, I., and
1195 Heinold, B.: Modelling emission and transport of key components of primary marine organic aerosol using the global aerosol-
1196 climate model ECHAM6.3-HAM2.3, *Geoscientific Model Development*, 18, 4183–4213, <https://doi.org/10.5194/gmd-18-4183-2025>, 2025.

- 1198 Li, J., Han, Z., Fu, P., Yao, X., and Liang, M.: Seasonal characteristics of emission, distribution, and radiative effect of marine
1199 organic aerosols over the western Pacific Ocean: an investigation with a coupled regional climate aerosol model, *Atmospheric*
1200 *Chemistry and Physics*, 24, 3129–3161, <https://doi.org/10.5194/acp-24-3129-2024>, 2024.
- 1201 Lohmann, U. and Feichter, J.: Global indirect aerosol effects: a review, *Atmospheric Chemistry and Physics*, 5, 715–737,
1202 <https://doi.org/10.5194/acp-5-715-2005>, 2005.
- 1203 Macke, A. and Flores, H.: The Expeditions PS106/1 and 2 of the Research Vessel POLARSTERN to the Arctic Ocean in 2017,
1204 Bremerhaven, Germany, 171 pp., https://doi.org/10.2312/BzPM_0719_2018, 2018.
- 1205 Madry, W. L., Toon, O. B., and O’Dowd, C. D.: Modeled optical thickness of sea-salt aerosol, *Journal of Geophysical Research:*
1206 *Atmospheres*, 116, <https://doi.org/10.1029/2010JD014691>, 2011.
- 1207 Malfatti, F., Lee, C., Tinta, T., Pendergraft, M. A., Celussi, M., Zhou, Y., Sultana, C. M., Rotter, A., Axson, J. L., Collins, D. B.,
1208 Santander, M. V., Anides Morales, A. L., Aluwihare, L. I., Riemer, N., Grassian, V. H., Azam, F., and Prather, K. A.: Detection of
1209 Active Microbial Enzymes in Nascent Sea Spray Aerosol: Implications for Atmospheric Chemistry and Climate, *Environ. Sci.*
1210 *Technol. Lett.*, 6, 171–177, <https://doi.org/10.1021/acs.estlett.8b00699>, 2019.
- 1211 Manders, A. M. M., Schaap, M., Querol, X., Albert, M. F. M. A., Vercauteren, J., Kuhlbusch, T. A. J., and Hoogerbrugge, R.: Sea
1212 salt concentrations across the European continent, *Atmospheric Environment*, 44, 2434–2442,
1213 <https://doi.org/10.1016/j.atmosenv.2010.03.028>, 2010.
- 1214 Matulová, M., Husárová, S., Capek, P., Sancelme, M., and Delort, A.-M.: Biotransformation of Various Saccharides and
1215 Production of Exopolymeric Substances by Cloud-Borne *Bacillus* sp. 3B6, *Environ. Sci. Technol.*, 48, 14238–14247,
1216 <https://doi.org/10.1021/es501350s>, 2014.
- 1217 Maturilli, M.: Continuous meteorological observations at station Ny-Ålesund (2011-08 et seq), Alfred Wegener Institute -
1218 Research Unit Potsdam, <https://doi.org/10.1594/PANGAEA.914979>, 2020.
- 1219 Maturilli, M., Herber, A., and König-Langlo, G.: Climatology and time series of surface meteorology in Ny-Ålesund, Svalbard,
1220 *Earth System Science Data*, 5, 155–163, <https://doi.org/10.5194/essd-5-155-2013>, 2013.
- 1221 Maturilli, M., Herber, A., and König-Langlo, G.: Surface radiation climatology for Ny-Ålesund, Svalbard (78.9° N), basic
1222 observations for trend detection, *Theor Appl Climatol*, 120, 331–339, <https://doi.org/10.1007/s00704-014-1173-4>, 2015.
- 1223 Mayot, N., Matrai, P., Ellingsen, I. H., Steele, M., Johnson, K., Riser, S. C., and Swift, D.: Assessing Phytoplankton Activities in
1224 the Seasonal Ice Zone of the Greenland Sea Over an Annual Cycle, *Journal of Geophysical Research: Oceans*, 123, 8004–8025,
1225 <https://doi.org/10.1029/2018JC014271>, 2018.
- 1226 McNeill, V. F.: Aqueous Organic Chemistry in the Atmosphere: Sources and Chemical Processing of Organic Aerosols, *Environ.*
1227 *Sci. Technol.*, 49, 1237–1244, <https://doi.org/10.1021/es5043707>, 2015.
- 1228 Mirrielees, J. A., Kirpes, R. M., Costa, E. J., Porter, G. C. E., Murray, B. J., Lata, N. N., Boschi, V., China, S., Grannas, A. M., Ault,
1229 A. P., Matrai, P. A., and Pratt, K. A.: Marine aerosol generation experiments in the High Arctic during summertime, *Elementa:*
1230 *Science of the Anthropocene*, 12, 00134, <https://doi.org/10.1525/elementa.2023.00134>, 2024.
- 1231 Müller, K., Lehmann, S., Pinxteren, D. van, Gnauk, T., Niedermeier, N., Wiedensohler, A., and Herrmann, H.: Particle
1232 characterization at the Cape Verde atmospheric observatory during the 2007 RHaMBLe intensive, *Atmospheric Chemistry*
1233 *and Physics*, 10, 2709–2721, <https://doi.org/10.5194/acp-10-2709-2010>, 2010.
- 1234 Neuwirth, E.: RColorBrewer: ColorBrewer Palettes, R package version 1.1-3, 2022.
- 1235 Nomokonova, T., Ebell, K., Löhnert, U., Maturilli, M., Ritter, C., and O’Connor, E.: Statistics on clouds and their relation to
1236 thermodynamic conditions at Ny-Ålesund using ground-based sensor synergy, *Atmospheric Chemistry and Physics*, 19, 4105–
1237 4126, <https://doi.org/10.5194/acp-19-4105-2019>, 2019.
- 1238 O’Dowd, C. D. and de Leeuw, G.: Marine aerosol production: a review of the current knowledge, *Philos Trans A Math Phys*
1239 *Eng Sci*, 365, 1753–1774, <https://doi.org/10.1098/rsta.2007.2043>, 2007.
- 1240 O’Dowd, C. D., Smith, M. H., Consterdine, I. E., and Lowe, J. A.: Marine aerosol, sea-salt, and the marine sulphur cycle: a short
1241 review, *Atmospheric Environment*, 31, 73–80, [https://doi.org/10.1016/S1352-2310\(96\)00106-9](https://doi.org/10.1016/S1352-2310(96)00106-9), 1997.
- 1242 Ooki, A., Uematsu, M., Miura, K., and Nakae, S.: Sources of sodium in atmospheric fine particles, *Atmospheric Environment*,
1243 36, 4367–4374, [https://doi.org/10.1016/S1352-2310\(02\)00341-2](https://doi.org/10.1016/S1352-2310(02)00341-2), 2002.
- 1244 Orellana, M. V. and Leck, C.: Chapter 9 - Marine Microgels, in: *Biogeochemistry of Marine Dissolved Organic Matter (Second*
1245 *Edition)*, edited by: Hansell, D. A. and Carlson, C. A., Academic Press, Boston, 451–480, <https://doi.org/10.1016/B978-0-12-405940-5.00009-1>, 2015.
- 1247 Orellana, M. V., Matrai, P. A., Leck, C., Rauschenberg, C. D., Lee, A. M., and Coz, E.: Marine microgels as a source of cloud
1248 condensation nuclei in the high Arctic, *PNAS*, 108, 13612–13617, <https://doi.org/10.1073/pnas.1102457108>, 2011.
- 1249 Oziel, L., Schourup-Kristensen, V., Wekerle, C., and Hauck, J.: The Pan-Arctic Continental Slope as an Intensifying Conveyor
1250 Belt for Nutrients in the Central Arctic Ocean (1985–2015), *Global Biogeochemical Cycles*, 36, e2021GB007268,
1251 <https://doi.org/10.1029/2021GB007268>, 2022.

- 1252 Panagiotopoulos, C. and Sempéré, R.: Analytical methods for the determination of sugars in marine samples: A historical
1253 perspective and future directions, *Limnology and Oceanography: Methods*, 3, 419–454,
1254 <https://doi.org/10.4319/lom.2005.3.419>, 2005.
- 1255 Penner, J. E., Andreae, M. O., Annegarn, H., Barrie, L., Feichter, J., Hegg, D., Jayaraman, A., Leaitch, R., Murphy, D., Nganga,
1256 J., and Pitari, G.: Aerosols, their Direct and Indirect Effects, *Climate Change 2001: The Scientific Basis. Contribution of Working
1257 Group I to the Third Assessment Report of the Intergovernmental Panel on Climate Change*, 289–348, 2001.
- 1258 Pierce, D.: *ncdf4: Interface to Unidata netCDF (Version 4 or Earlier) Format Data*, R package version 1.22, 2023.
- 1259 Pilinis, C., Pandis, S. N., and Seinfeld, J. H.: Sensitivity of direct climate forcing by atmospheric aerosols to aerosol size and
1260 composition, *Journal of Geophysical Research*, 100, 18,739–18,754, <https://doi.org/10.1029/95JD02119>, 1995.
- 1261 Pilz, C., Düsing, S., Wehner, B., Müller, T., Siebert, H., Voigtländer, J., and Lonardi, M.: CAMP: an instrumented platform for
1262 balloon-borne aerosol particle studies in the lower atmosphere, *Atmospheric Measurement Techniques*, 15, 6889–6905,
1263 <https://doi.org/10.5194/amt-15-6889-2022>, 2022.
- 1264 Pilz, C., Lonardi, M., Egerer, U., Siebert, H., Ehrlich, A., Heymsfield, A. J., Schmitt, C. G., Shupe, M. D., Wehner, B., and
1265 Wendisch, M.: Profile observations of the Arctic atmospheric boundary layer with the BELUGA tethered balloon during
1266 MOSAiC, *Sci Data*, 10, 534, <https://doi.org/10.1038/s41597-023-02423-5>, 2023.
- 1267 Pilz, C., Cassano, J. J., de Boer, G., Kirbus, B., Lonardi, M., Pöhlker, M., Shupe, M. D., Siebert, H., Wendisch, M., and Wehner,
1268 B.: Tethered balloon measurements reveal enhanced aerosol occurrence aloft interacting with Arctic low-level clouds,
1269 *Elementa: Science of the Anthropocene*, 12, 00120, <https://doi.org/10.1525/elementa.2023.00120>, 2024.
- 1270 van Pinxteren, M., Müller, C., Iinuma, Y., Stolle, C., and Herrmann, H.: Chemical Characterization of Dissolved Organic
1271 Compounds from Coastal Sea Surface Microlayers (Baltic Sea, Germany), *Environmental Science & Technology*, 46, 10455–
1272 10462, <https://doi.org/10.1021/es204492b>, 2012.
- 1273 van Pinxteren, M., Barthel, S., Fomba, K. W., Müller, K., Von Tümpling, W., and Herrmann, H.: The influence of environmental
1274 drivers on the enrichment of organic carbon in the sea surface microlayer and in submicron aerosol particles – measurements
1275 from the Atlantic Ocean, *Elem Sci Anth*, 5, 1–21, <https://doi.org/10.1525/elementa.225>, 2017.
- 1276 van Pinxteren, M., Robinson, T.-B., Zeppenfeld, S., Gong, X., Bahlmann, E., Fomba, K. W., Triesch, N., Stratmann, F., Wurl, O.,
1277 Engel, A., Wex, H., and Herrmann, H.: High number concentrations of transparent exopolymer particles in ambient aerosol
1278 particles and cloud water – a case study at the tropical Atlantic Ocean, *Atmospheric Chemistry and Physics*, 22, 5725–5742,
1279 <https://doi.org/10.5194/acp-22-5725-2022>, 2022.
- 1280 van Pinxteren, M., Zeppenfeld, S., Fomba, K. W., Triesch, N., Frka, S., and Herrmann, H.: Amino acids, carbohydrates, and
1281 lipids in the tropical oligotrophic Atlantic Ocean: sea-to-air transfer and atmospheric in situ formation, *Atmospheric Chemistry
1282 and Physics*, 23, 6571–6590, <https://doi.org/10.5194/acp-23-6571-2023>, 2023.
- 1283 Platt, S. M., Hov, Ø., Berg, T., Breivik, K., Eckhardt, S., Eleftheriadis, K., Evangelidou, N., Fiebig, M., Fisher, R., Hansen, G.,
1284 Hansson, H.-C., Heintzenberg, J., Hermansen, O., Heslin-Rees, D., Holmén, K., Hudson, S., Kallenborn, R., Krejci, R., Krognes,
1285 T., Larssen, S., Lowry, D., Lund Myhre, C., Lunder, C., Nisbet, E., Nizzetto, P. B., Park, K.-T., Pedersen, C. A., Aspö Pfaffhuber,
1286 K., Röckmann, T., Schmidbauer, N., Solberg, S., Stohl, A., Ström, J., Svendby, T., Tunved, P., Tørnkvist, K., van der Veen, C.,
1287 Vratolis, S., Yoon, Y. J., Yttri, K. E., Zieger, P., Aas, W., and Tørseth, K.: Atmospheric composition in the European Arctic and
1288 30 years of the Zeppelin Observatory, Ny-Ålesund, *Atmospheric Chemistry and Physics*, 22, 3321–3369,
1289 <https://doi.org/10.5194/acp-22-3321-2022>, 2022.
- 1290 van de Poll, W. H., Maat, D. S., Fischer, P., Visser, R. J. W., Brussaard, C. P. D., and Buma, A. G. J.: Solar radiation and solar
1291 radiation driven cycles in warming and freshwater discharge control seasonal and inter-annual phytoplankton chlorophyll a
1292 and taxonomic composition in a high Arctic fjord (Kongsfjorden, Spitsbergen), *Limnology and Oceanography*, 66, 1221–1236,
1293 <https://doi.org/10.1002/lno.11677>, 2021.
- 1294 Porter, G. C. E., Adams, M. P., Brooks, I. M., Ickes, L., Karlsson, L., Leck, C., Salter, M. E., Schmale, J., Siegel, K., Sikora, S. N. F.,
1295 Tarn, M. D., Vüllers, J., Wernli, H., Zieger, P., Zinke, J., and Murray, B. J.: Highly Active Ice-Nucleating Particles at the Summer
1296 North Pole, *Journal of Geophysical Research: Atmospheres*, 127, e2021JD036059, <https://doi.org/10.1029/2021JD036059>,
1297 2022.
- 1298 Quinn, P. K., Collins, D. B., Grassian, V. H., Prather, K. A., and Bates, T. S.: Chemistry and Related Properties of Freshly Emitted
1299 Sea Spray Aerosol, *Chemical Reviews*, 115, 4383–4399, <https://doi.org/10.1021/cr500713g>, 2015.
- 1300 Ramasamy, K. P., Mahawar, L., Rajasabapathy, R., Rajeshwari, K., Miceli, C., and Pucciarelli, S.: Comprehensive insights on
1301 environmental adaptation strategies in Antarctic bacteria and biotechnological applications of cold adapted molecules, *Front.
1302 Microbiol.*, 14, <https://doi.org/10.3389/fmicb.2023.1197797>, 2023.
- 1303 Rinaldi, M., Decesari, S., Carbone, C., Finessi, E., Fuzzi, S., Ceburnis, D., O’Dowd, C. D., Sciare, J., Burrows, J. P., Vrekoussis, M.,
1304 Ervens, B., Tsigaridis, K., and Facchini, M. C.: Evidence of a natural marine source of oxalic acid and a possible link to glyoxal,
1305 *Journal of Geophysical Research: Atmospheres*, 116, <https://doi.org/10.1029/2011JD015659>, 2011.
- 1306 Robinson, T.-B., Stolle, C., and Wurl, O.: Depth is relative: the importance of depth for transparent exopolymer particles in
1307 the near-surface environment, *Ocean Science*, 15, 1653–1666, <https://doi.org/10.5194/os-15-1653-2019>, 2019a.

- 1308 Robinson, T.-B., Wurl, O., Bahlmann, E., Jürgens, K., and Stolle, C.: Rising bubbles enhance the gelatinous nature of the air–
1309 sea interface, *Limnology and Oceanography*, 64, 2358–2372, <https://doi.org/10.1002/lno.11188>, 2019b.
- 1310 Rocchi, A., von Jackowski, A., Welti, A., Li, G., Kanji, Z. A., Povozhnyy, V., Engel, A., Schmale, J., Nenes, A., Berdalet, E., Simó,
1311 R., and Dall’Osto, M.: Glucose Enhances Salinity-Driven Sea Spray Aerosol Production in Eastern Arctic Waters, *Environ. Sci.*
1312 *Technol.*, 58, 8748–8759, <https://doi.org/10.1021/acs.est.4c02826>, 2024.
- 1313 Russell, L. M., Hawkins, L. N., Frossard, A. A., Quinn, P. K., and Bates, T. S.: Carbohydrate-like composition of submicron
1314 atmospheric particles and their production from ocean bubble bursting, *Proc. Natl. Acad. Sci. U.S.A.*, 107, 6652–6657,
1315 <https://doi.org/10.1073/pnas.0908905107>, 2010.
- 1316 Sander, R., Keene, W. C., Pszenny, A. a. P., Arimoto, R., Ayers, G. P., Baboukas, E., Caine, J. M., Crutzen, P. J., Duce, R. A.,
1317 Hönninger, G., Huebert, B. J., Maenhaut, W., Mihalopoulos, N., Turekian, V. C., and Van Dingenen, R.: Inorganic bromine in
1318 the marine boundary layer: a critical review, *Atmospheric Chemistry and Physics*, 3, 1301–1336, <https://doi.org/10.5194/acp-3-1301-2003>, 2003.
- 1320 Šantl-Temkiv, T., Gosewinkel, U., Starnawski, P., Lever, M., and Finster, K.: Aeolian dispersal of bacteria in southwest
1321 Greenland: their sources, abundance, diversity and physiological states, *FEMS Microbiol Ecol*, 94,
1322 <https://doi.org/10.1093/femsec/fiy031>, 2018.
- 1323 Šantl-Temkiv, T., Amato, P., Casamayor, E. O., Lee, P. K. H., and Pointing, S. B.: Microbial ecology of the atmosphere, *FEMS*
1324 *Microbiology Reviews*, 46, fuac009, <https://doi.org/10.1093/femsre/fuac009>, 2022.
- 1325 Schartau, M., Engel, A., Schröter, J., Thoms, S., Völker, C., and Wolf-Gladrow, D.: Modelling carbon overconsumption and the
1326 formation of extracellular particulate organic carbon, *Biogeosciences*, 4, 433–454, <https://doi.org/10.5194/bg-4-433-2007>,
1327 2007.
- 1328 Schill, S. R., Burrows, S. M., Hasenecz, E. S., Stone, E. A., and Bertram, T. H.: The Impact of Divalent Cations on the Enrichment
1329 of Soluble Saccharides in Primary Sea Spray Aerosol, *Atmosphere*, 9, 476, <https://doi.org/10.3390/atmos9120476>, 2018.
- 1330 Schmale, J., Zieger, P., and Ekman, A. M. L.: Aerosols in current and future Arctic climate, *Nature Climate Change*, 11, 95–105,
1331 <https://doi.org/10.1038/s41558-020-00969-5>, 2021.
- 1332 Schmale, J., Sharma, S., Decesari, S., Pernov, J., Massling, A., Hansson, H.-C., von Salzen, K., Skov, H., Andrews, E., Quinn, P.
1333 K., Upchurch, L. M., Eleftheriadis, K., Traversi, R., Gilardoni, S., Mazzola, M., Laing, J., and Hopke, P.: Pan-Arctic seasonal cycles
1334 and long-term trends of aerosol properties from 10 observatories, *Atmospheric Chemistry and Physics*, 22, 3067–3096,
1335 <https://doi.org/10.5194/acp-22-3067-2022>, 2022.
- 1336 Sharma, S., Barrie, L. a., Magnusson, E., Brattström, G., Leaitch, W. r., Steffen, A., and Landsberger, S.: A Factor and Trends
1337 Analysis of Multidecadal Lower Tropospheric Observations of Arctic Aerosol Composition, Black Carbon, Ozone, and Mercury
1338 at Alert, Canada, *Journal of Geophysical Research: Atmospheres*, 124, 14133–14161, <https://doi.org/10.1029/2019JD030844>,
1339 2019.
- 1340 Shestakova, A., Chechin, D., Lüpkes, C., Hartmann, J., and Maturilli, M.: Foehn effect during easterly flow over Svalbard,
1341 <https://doi.org/10.5194/acp-2021-478>, 2021.
- 1342 Simon, D. J., Hartmann, J., Schaefer, J., Zeppenfeld, S., Lüpkes, C., Hartmann, M., Wetzel, B., Heinold, B., Jurányi, Z., Schulz,
1343 A., Köhler, L., Jörss, A.-M., Herber, A., Henning, S., Pöhlker, M. L., Roberts, G. C., and Stratmann, F.: Turbulent aerosol fluxes
1344 from airborne measurements over the Arctic Ocean, *Geophys. Res. Lett.*, 52, e2025GL117094,
1345 <https://doi.org/10.1029/2025GL117094>, 2025
- 1346 Sinreich, R., Coburn, S., Dix, B., and Volkamer, R.: Ship-based detection of glyoxal over the remote tropical Pacific Ocean,
1347 *Atmospheric Chemistry and Physics*, 10, 11359–11371, <https://doi.org/10.5194/acp-10-11359-2010>, 2010.
- 1348 Sorooshian, A., Lu, M.-L., Brechtel, F. J., Jonsson, H., Feingold, G., Flagan, R. C., and Seinfeld, J. H.: On the Source of Organic
1349 Acid Aerosol Layers above Clouds, *Environ. Sci. Technol.*, 41, 4647–4654, <https://doi.org/10.1021/es0630442>, 2007.
- 1350 Stein, A. F., Draxler, R. R., Rolph, G. D., Stunder, B. J. B., Cohen, M. D., and Ngan, F.: NOAA’s HYSPLIT Atmospheric Transport
1351 and Dispersion Modeling System, *Bull. Amer. Meteor. Soc.*, 96, 2059–2077, <https://doi.org/10.1175/BAMS-D-14-00110.1>,
1352 2015.
- 1353 Struthers, H., Ekman, A. M. L., Glantz, P., Iversen, T., Kirkevåg, A., Mårtensson, E. M., Seland, Ø., and Nilsson, E. D.: The effect
1354 of sea ice loss on sea salt aerosol concentrations and the radiative balance in the Arctic, *Atmospheric Chemistry and Physics*,
1355 11, 3459–3477, <https://doi.org/10.5194/acp-11-3459-2011>, 2011.
- 1356 Su, B., Bi, X., Zhang, Z., Liang, Y., Song, C., Wang, T., Hu, Y., Li, L., Zhou, Z., Yan, J., Wang, X., and Zhang, G.: Enrichment of
1357 calcium in sea spray aerosol: insights from bulk measurements and individual particle analysis during the R/V *Xuelong* cruise
1358 in the summertime in Ross Sea, Antarctica, *Atmospheric Chemistry and Physics*, 23, 10697–10711,
1359 <https://doi.org/10.5194/acp-23-10697-2023>, 2023.
- 1360 Theodosi, C., Im, U., Bougiatioti, A., Zarpas, P., Yenigun, O., and Mihalopoulos, N.: Aerosol chemical composition over
1361 Istanbul, *Science of The Total Environment*, 408, 2482–2491, <https://doi.org/10.1016/j.scitotenv.2010.02.039>, 2010.

- 1362 Thyng, K., Greene, C. A., Hetland, R. D., Zimmerle, H. M., and DiMarco, S.: True colors of oceanography: Guidelines for effective
1363 and accurate colormap selection, *Oceanography*, 3, <https://doi.org/10.5670/oceanog.2016.66>, 2016.
- 1364 Tilgner, A. and Herrmann, H.: Radical-driven carbonyl-to-acid conversion and acid degradation in tropospheric aqueous
1365 systems studied by CAPRAM, *Atmospheric Environment*, 44, 5415–5422, <https://doi.org/10.1016/j.atmosenv.2010.07.050>,
1366 2010.
- 1367 Tørseth, K., Aas, W., Breivik, K., Fjæraa, A. M., Fiebig, M., Hjellbrekke, A. G., Lund Myhre, C., Solberg, S., and Yttri, K. E.:
1368 Introduction to the European Monitoring and Evaluation Programme (EMEP) and observed atmospheric composition change
1369 during 1972–2009, *Atmospheric Chemistry and Physics*, 12, 5447–5481, <https://doi.org/10.5194/acp-12-5447-2012>,
1370 2012.
- 1371 Trainic, M., Koren, I., Sharoni, S., Frada, M., Segev, L., Rudich, Y., and Vardi, A.: Infection Dynamics of a Bloom-Forming Alga
1372 and Its Virus Determine Airborne Coccolith Emission from Seawater, *iScience*, 6, 327–335,
1373 <https://doi.org/10.1016/j.isci.2018.07.017>, 2018.
- 1374 Triesch, N., van Pinxteren, M., Engel, A., and Herrmann, H.: Concerted measurements of free amino acids at the Cabo Verde
1375 islands: high enrichments in submicron sea spray aerosol particles and cloud droplets, *Atmospheric Chemistry and Physics*,
1376 21, 163–181, <https://doi.org/10.5194/acp-21-163-2021>, 2021.
- 1377 Turekian, V. C., Macko, S. A., and Keene, W. C.: Concentrations, isotopic compositions, and sources of size-resolved,
1378 particulate organic carbon and oxalate in near-surface marine air at Bermuda during spring, *Journal of Geophysical Research: Atmospheres*,
1379 108, <https://doi.org/10.1029/2002JD002053>, 2003.
- 1380 Veron, F.: Ocean Spray, *Annual Review of Fluid Mechanics*, 47, 507–538, <https://doi.org/10.1146/annurev-fluid-010814-014651>, 2015.
- 1382 Vihtakari, M.: PlotSvalbard: PlotSvalbard-Plot research data from Svalbard on maps, R package version 0.9 2, 2020.
- 1383 Warneck, P.: In-cloud chemistry opens pathway to the formation of oxalic acid in the marine atmosphere, *Atmospheric Environment*,
1384 37, 2423–2427, [https://doi.org/10.1016/S1352-2310\(03\)00136-5](https://doi.org/10.1016/S1352-2310(03)00136-5), 2003.
- 1385 Wendisch, M., Brückner, M., Burrows, J. P., Crewell, S., Dethloff, K., Ebell, K., Lüpkes, C., Macke, A., Notholt, J., and Quaas, J.:
1386 Understanding causes and effects of rapid warming in the Arctic, *Eos*, 98, 2017.
- 1387 Wendisch, M., Macke, A., Ehrlich, A., Lüpkes, C., Mech, M., Chechin, D., Dethloff, K., Barrientos, C., Bozem, H., Brückner, M.,
1388 Clemen, H.-C., Crewell, S., Donth, T., Dupuy, R., Ebell, K., Egerer, U., Engelmann, R., Engler, C., Eppers, O., Gehrmann, M.,
1389 Gong, X., Gottschalk, M., Gourbeyre, C., Griesche, H., Hartmann, J., Hartmann, M., Heinold, B., Herber, A., Herrmann, H.,
1390 Heygster, G., Hoor, P., Jafariserajehlou, S., Jäkel, E., Järvinen, E., Jourdan, O., Kästner, U., Kecorius, S., Knudsen, E. M., Köllner,
1391 F., Kretzschmar, J., Lelli, L., Leroy, D., Maturilli, M., Mei, L., Mertens, S., Mioche, G., Neuber, R., Nicolaus, M., Nomokonova, T.,
1392 Notholt, J., Palm, M., van Pinxteren, M., Quaas, J., Richter, P., Ruiz-Donoso, E., Schäfer, M., Schmieder, K., Schnaiter, M.,
1393 Schneider, J., Schwarzenböck, A., Seifert, P., Shupe, M. D., Siebert, H., Spreen, G., Stapf, J., Stratmann, F., Vogl, T., Welti, A.,
1394 Wex, H., Wiedensohler, A., Zanatta, M., and Zeppenfeld, S.: The Arctic Cloud Puzzle: Using ALOUD/PASCAL Multi-Platform
1395 Observations to Unravel the Role of Clouds and Aerosol Particles in Arctic Amplification, *Bull. Amer. Meteor. Soc.*,
1396 <https://doi.org/10.1175/BAMS-D-18-0072.1>, 2018.
- 1397 Wendisch, M., Brückner, M., Crewell, S., Ehrlich, A., Notholt, J., Lüpkes, C., Macke, A., Burrows, J. P., Rinke, A., Quaas, J.,
1398 Maturilli, M., Schemann, V., Shupe, M. D., Akansu, E. F., Barrientos-Velasco, C., Bärfuss, K., Blechschmidt, A.-M., Block, K.,
1399 Bougoudis, I., Bozem, H., Böckmann, C., Bracher, A., Bresson, H., Bretschneider, L., Buschmann, M., Chechin, D. G., Chylik, J.,
1400 Dahlke, S., Deneke, H., Dethloff, K., Donth, T., Dorn, W., Dupuy, R., Ebell, K., Egerer, U., Engelmann, R., Eppers, O., Gerdes, R.,
1401 Gierens, R., Gorodetskaya, I. V., Gottschalk, M., Griesche, H., Gryanik, V. M., Handorf, D., Harm-Altstädter, B., Hartmann, J.,
1402 Hartmann, M., Heinold, B., Herber, A., Herrmann, H., Heygster, G., Höschel, I., Hofmann, Z., Hölemann, J., Hünnerbein, A.,
1403 Jafariserajehlou, S., Jäkel, E., Jacobi, C., Janout, M., Jansen, F., Jourdan, O., Jurányi, Z., Kalesse-Los, H., Kanzow, T., Käthner,
1404 R., Kliesch, L. L., Klingebiel, M., Knudsen, E. M., Kovács, T., Körtke, W., Krampe, D., Kretzschmar, J., Kreyling, D., Kulla, B.,
1405 Kunkel, D., Lampert, A., Lauer, M., Lelli, L., Lerber, A. von, Linke, O., Löhnert, U., Lonardi, M., Losa, S. N., Losch, M., Maahn,
1406 M., Mech, M., Mei, L., Mertens, S., Metzner, E., Mewes, D., Michaelis, J., Mioche, G., Moser, M., Nakoudi, K., Neggers, R.,
1407 Neuber, R., Nomokonova, T., Oelker, J., Papakonstantinou-Presvelou, I., et al.: Atmospheric and Surface Processes, and
1408 Feedback Mechanisms Determining Arctic Amplification: A Review of First Results and Prospects of the (AC)3 Project, *Bulletin*
1409 *of the American Meteorological Society*, 104, E208–E242, <https://doi.org/10.1175/BAMS-D-21-0218.1>, 2023.
- 1410 White, W. H.: Chemical markers for sea salt in IMPROVE aerosol data, *Atmospheric Environment*, 42, 261–274,
1411 <https://doi.org/10.1016/j.atmosenv.2007.09.040>, 2008.
- 1412 Wickham, H.: Reshaping Data with the reshape Package, *Journal of Statistical Software*, 21, 1–20, 2007.
- 1413 Wickham, H.: ggplot2: Elegant Graphics for Data Analysis, Springer-Verlag New York, https://doi.org/10.1007/978-3-319-24277-4_2, 2016.
- 1415 Wickham, H., François, R., Henry, L., Müller, K., and Vaughan, D.: dplyr: A Grammar of Data Manipulation, R package version
1416 1.1.4, 2023a.
- 1417 Wickham, H., Pedersen, T. L., and Seidel, D.: scales: Scale Functions for Visualization, R package version 1.3.0, 2023b.

- 1418 Wietz, M., Engel, A., Ramondenc, S., Niwano, M., von Appen, W.-J., Priest, T., von Jackowski, A., Metfies, K., Bienhold, C., and
 1419 Boetius, A.: The Arctic summer microbiome across Fram Strait: Depth, longitude, and substrate concentrations structure
 1420 microbial diversity in the euphotic zone, *Environmental Microbiology*, 26, e16568, [https://doi.org/10.1111/1462-](https://doi.org/10.1111/1462-2920.16568)
 1421 2920.16568, 2024.
- 1422 Wietz, M., van Pinxteren, M., Freese, H. M., Sproer, C., and Zeppenfeld, S.: Seasonal connectivity of microbes and
 1423 carbohydrates between ocean, atmosphere, and cryosphere in Kongsfjorden (Svalbard, Arctic Ocean), preprint,
 1424 <https://doi.org/10.64898/2025.12.01.691664>, uploaded on 2 December 2025.
- 1425 Willis, M. D., Leaitch, W. R., and Abbatt, J. P. D.: Processes Controlling the Composition and Abundance of Arctic Aerosol,
 1426 *Reviews of Geophysics*, 56, 621–671, <https://doi.org/10.1029/2018RG000602>, 2018.
- 1427 Wong, J. P. S., Tsagkaraki, M., Tsiodra, I., Mihalopoulos, N., Violaki, K., Kanakidou, M., Sciare, J., Nenes, A., and Weber, R. J.:
 1428 Effects of Atmospheric Processing on the Oxidative Potential of Biomass Burning Organic Aerosols, *Environ. Sci. Technol.*, 53,
 1429 6747–6756, <https://doi.org/10.1021/acs.est.9b01034>, 2019.
- 1430 Wurl, O. and Holmes, M.: The gelatinous nature of the sea-surface microlayer, *Marine Chemistry*, 110, 89–97,
 1431 <https://doi.org/10.1016/j.marchem.2008.02.009>, 2008.
- 1432 Xu, W., Ovadnevaite, J., Fossum, K. N., Lin, C., Huang, R.-J., Ceburnis, D., and O’Dowd, C.: Sea spray as an obscured source for
 1433 marine cloud nuclei, *Nat. Geosci.*, 15, 282–286, <https://doi.org/10.1038/s41561-022-00917-2>, 2022.
- 1434 Yang, C., Zhou, S., Zhang, C., Yu, M., Cao, F., and Zhang, Y.: Atmospheric Chemistry of Oxalate: Insight Into the Role of Relative
 1435 Humidity and Aerosol Acidity From High-Resolution Observation, *Journal of Geophysical Research: Atmospheres*, 127,
 1436 e2021JD035364, <https://doi.org/10.1029/2021JD035364>, 2022.
- 1437 Yttri, K. E., Bäcklund, A., Conen, F., Eckhardt, S., Evangelidou, N., Fiebig, M., Kasper-Giebl, A., Gold, A., Gundersen, H., Myhre,
 1438 C. L., Platt, S. M., Simpson, D., Surratt, J. D., Szidat, S., Rauber, M., Tørseth, K., Ytre-Eide, M. A., Zhang, Z., and Aas, W.:
 1439 Composition and sources of carbonaceous aerosol in the European Arctic at Zeppelin Observatory, Svalbard (2017 to 2020),
 1440 *Atmospheric Chemistry and Physics*, 24, 2731–2758, <https://doi.org/10.5194/acp-24-2731-2024>, 2024.
- 1441 Yu, H., Kaufman, Y. J., Chin, M., Feingold, G., Remer, L. A., Anderson, T. L., Balkanski, Y., Bellouin, N., Boucher, O., Christopher,
 1442 S., DeCola, P., Kahn, R., Koch, D., Loeb, N., Reddy, M. S., Schulz, M., Takemura, T., and Zhou, M.: A review of measurement-
 1443 based assessments of the aerosol direct radiative effect and forcing, *Atmospheric Chemistry and Physics*, 6, 613–666,
 1444 <https://doi.org/10.5194/acp-6-613-2006>, 2006.
- 1445 Zäncker, B., Cunliffe, M., and Engel, A.: Eukaryotic community composition in the sea surface microlayer across an east–west
 1446 transect in the Mediterranean Sea, *Biogeosciences*, 18, 2107–2118, <https://doi.org/10.5194/bg-18-2107-2021>, 2021.
- 1447 Zeising, M., Oziel, L., Thoms, S., Gürses, Ö., Hauck, J., Heinold, B., Losa, S. N., van Pinxteren, M., Völker, C., Zeppenfeld, S., and
 1448 Bracher, A.: Assessment of transparent exopolymer particles in the Arctic Ocean implemented into the coupled ocean–sea
 1449 ice–biogeochemistry model FESOM2.1–REcoM3, *Geoscientific Model Development*, 19, 2077–2109,
 1450 <https://doi.org/10.5194/gmd-19-2077-2026>, 2026.
- 1451 Zeppenfeld, S. and Schmidt, L.: Dissolved and particulate carbohydrates and inorganic ions in the sea surface microlayer and
 1452 bulk water of Kongsfjorden (Autumn 2021/Spring 2022), <https://doi.org/10.1594/PANGAEA.982606>, 2025.
- 1453 Zeppenfeld, S., van Pinxteren, M., Engel, A., and Herrmann, H.: A protocol for quantifying mono- and polysaccharides in
 1454 seawater and related saline matrices by electro-dialysis (ED) – combined with HPAEC-PAD, *Ocean Science*, 16, 817–830,
 1455 <https://doi.org/10.5194/os-16-817-2020>, 2020.
- 1456 Zeppenfeld, S., van Pinxteren, M., van Pinxteren, D., Wex, H., Berdalet, E., Vaqué, D., Dall’Osto, M., and Herrmann, H.: Aerosol
 1457 Marine Primary Carbohydrates and Atmospheric Transformation in the Western Antarctic Peninsula, *ACS Earth Space Chem.*,
 1458 5, 1032–1047, <https://doi.org/10.1021/acsearthspacechem.0c00351>, 2021.
- 1459 Zeppenfeld, S., van Pinxteren, M., Hartmann, M., Zeising, M., Bracher, A., and Herrmann, H.: Marine carbohydrates in Arctic
 1460 aerosol particles and fog – diversity of oceanic sources and atmospheric transformations, *Atmospheric Chemistry and Physics*,
 1461 23, 15561–15587, <https://doi.org/10.5194/acp-23-15561-2023>, 2023.
- 1462 Zeppenfeld, S., Schaefer, J., van Pinxteren, M., and Schmidt, L.: Marine combined carbohydrates and inorganic ions in
 1463 atmospheric total suspended particles across altitudes in the lower troposphere of Ny-Ålesund, Svalbard,
 1464 <https://doi.org/10.1594/PANGAEA.982703>, 2025.
- 1465 Zhou, S., Gonzalez, L., Leithead, A., Finewax, Z., Thalman, R., Vlasenko, A., Vagle, S., Miller, L. A., Li, S.-M., Bureekul, S.,
 1466 Furutani, H., Uematsu, M., Volkamer, R., and Abbatt, J.: Formation of gas-phase carbonyls from heterogeneous oxidation of
 1467 polyunsaturated fatty acids at the air–water interface and of the sea surface microlayer, *Atmospheric Chemistry and Physics*,
 1468 14, 1371–1384, <https://doi.org/10.5194/acp-14-1371-2014>, 2014.
- 1469 Zhu, B., Sun-Waterhouse, D., and You, L.: Insights into the mechanisms underlying the degradation of xylooligosaccharides in
 1470 UV/H₂O₂ system, *Carbohydrate Polymers*, 317, 121091, <https://doi.org/10.1016/j.carbpol.2023.121091>, 2023.

1471 Zhu, Y.-S., Connolly, A., Guyon, A., and FitzGerald, R. J.: Solubilisation of calcium and magnesium from the marine red algae
1472 *Lithothamnion calcareum*, *International Journal of Food Science and Technology*, 49, 1600–1606,
1473 <https://doi.org/10.1111/ijfs.12459>, 2014.